HHS Public Access

Author manuscript

Neuron. Author manuscript; available in PMC 2018 August 30.

Published in final edited form as:

Neuron. 2017 August 30; 95(5): 1089–1102.e5. doi:10.1016/j.neuron.2017.07.036.

Input-timing dependent plasticity in the hippocampal CA2 region and its potential role in social memory

Felix Leroy[1,*], **David H. Brann**[1], **Torcato Meira**[1,2,3], and **Steven A. Siegelbaum**[1,4,*]

[1]Neuroscience department, Kavli Brain Institute, Columbia University Medical Center, 1051 Riverside Drive, New York, NY 10032

[2]Life and Health Sciences Research Institute (ICVS), School of Medicine, University of Minho, Braga, Portugal

[3]ICVS/3B's, PT Government Associate Laboratory, Braga / Guimarães, Portugal

Summary

Input-timing dependent plasticity (ITDP) is a circuit-based synaptic learning rule whereby precisely timed, paired activation of direct entorhinal cortex (EC) and Schaffer collateral (SC) inputs to hippocampal CA1 pyramidal neurons (PNs) produces a long-term enhancement of CA1 SC excitation, which has been linked to specificity of contextual memory. We report that paired activation of EC and SC inputs also increases SC excitation of CA2 PNs, which are important for social memory. However, whereas CA1 ITDP depends on endocannabinoid CB1 receptor-dependent long-term depression of feedforward inhibition (iLTD) mediated by cholecystokinin-positive interneurons, CA2 ITDP depends on δ-opioid receptor-dependent iLTD of parvalbumin-positive interneuron inhibition. Blockade of CA2 δ-opioid receptors blocked ITDP and impaired social memory whereas a social encounter with a novel animal decreased CA2 feedforward inhibition and occluded ITDP. Thus, ITDP may provide a more general synaptic learning rule for distinct forms of hippocampal-dependent memory through its recruitment by distinct hippocampal regions.

Keywords

ITDP; CA2; delta opioid receptor; social memory

[*]Correspondence: sas8@columbia.edu (S.A.S) or felxfel@aol.com (F.L.).

[4]**Lead Contact:** Steven A. Siegelbaum sas8@columbia.edu

Author Contributions

Conceptualization, F.L. and S.A.S; Investigation, F.L., D.H.B and T.M.; F.L. performed intracellular recordings; F.L. and T.M. performed the behavioral assays; F.L. and D.H.B performed the IHC and viral injections; Writing – Original draft, F.L.; Writing – Review and editing, F.L. and S.A.S; Visualization, F.L.; Supervision, S.A.S; Funding acquisition, S.A.S.

Conflict of interest statement

The authors declare no conflicts of interest.

Introduction

Most studies of the role of long-term synaptic plasticity in learning and memory have focused on Hebbian plasticity, in which activity in a given excitatory pathway leads to homosynaptic changes in the activated synapses (Alger and Teyler, 1976; Bliss and Lomo, 1973). The induction of such forms of plasticity often requires strong, high-frequency tetanic stimulation, as in the induction of long-term potentiation of excitatory transmission at the Schaffer collateral (SC) synapses onto CA1 pyramidal neurons (PNs) in response to one or more bursts of 100 Hz tetanic stimulation. However, such prolonged high-frequency activation may not occur under physiological conditions, where hippocampal neuron firing tends to be sparse (Kowalski et al., 2015).

Heterosynaptic forms of plasticity, where activation of one input modulates the strength of a second inputs, provides another mechanism for altering the strength of synaptic transmission. These forms of plasticity have been described in various parts of the brain, including cerebellum (Ito, 2001; Safo and Regehr, 2008) and amygdala (Cho et al., 2011), with mechanisms that are often tuned to the particular properties of the given circuit. However, the importance of heterosynaptic forms of plasticity in the hippocampus has been less widely investigated.

Our laboratory described a circuit-based form of heterosynaptic plasticity, termed input-timing dependent plasticity (ITDP), in which low-frequency, paired activation of the direct entorhinal cortex (EC) inputs to CA1 PNs precisely 20 ms prior to SC input produces a long-term enhancement of SC-evoked excitation of CA1 (Basu et al., 2013; Dudman et al., 2007). The increase in the SC-evoked synaptic depolarization results from both long-term potentiation of the SC excitatory synaptic input (eLTP) and long-term depression of feed-forward inhibition (iLTD) mediated by cholecystokinin-expressing (CCK^+) interneurons (INs), which depends on activation of endocannabinoid CB1 receptors (Basu et al., 2013). Unlike LTP, ITDP is induced by weak sub-threshold paired stimuli at a low (1Hz) frequency observed during *in vivo* recordings (Csicsvari et al., 1999; Frank et al., 2001). Of particular interest, the ITDP pairing interval matches the delay line architecture inherent in the cortico-hippocampal circuit, in which information from EC arrives at CA1 through the direct path, approximately 15–20 ms prior to transmission through the indirect trisynaptic pathway (Yeckel and Berger, 1990). Thus, ITDP was proposed to assess the salience of the information relayed to a given CA1 PN through the trisynaptic path (EC→Dentate Gyrus→CA3→CA1) based on its temporal relation to sensory contextual information conveyed by the direct EC inputs. Indeed, a recent study suggests that CA1 ITDP may serve to enhance the specificity of contextual fear memory and the strength of object recognition memory (Basu et al., 2016).

One question raised by these previous findings is whether ITDP is specific to CA1 or whether it might serve as a more widespread synaptic learning rule. Here we have focused on plasticity mechanisms in the hippocampal CA2 region, which has recently shown to be important for social memory, the ability of an animal to recognize and remember a conspecific (Hitti and Siegelbaum, 2014; Stevenson and Caldwell, 2014). As CA2 PNs also receive direct input from EC and indirect input conveyed by the trisynaptic path

(EC→Dentate Gyrus→CA3→CA2), we investigated whether ITDP can be induced at CA2 PN synapses, and whether plasticity mechanisms related to ITDP may be associated with social memory.

Results

Electrical pairing of EC and SC CA2 inputs at a 20 ms interval induces ITDP

We first examined whether paired electrical stimulation of the EC and SC inputs was able to induce ITDP of either EC or SC excitation of CA2 PNs. We recorded from CA2 PNs in dorsal hippocampal slices, confirming neuronal identity by electrophysiological (Figure 1A1), morphological (Figure 1A2, 3F), and molecular properties (Figure 1A2, 4E3, 6E3, see Methods). One stimulating electrode was placed in the *stratum lacunosum-moleculare* (*SLM*) of CA1c, near the hippocampal fissure to activate the direct EC inputs with a second placed in the *stratum radiatum* (*SR*) of CA3 near the CA2 border to activate SC inputs (Figure 1B1), as described (Chevaleyre and Siegelbaum, 2010). Stimulating voltage intensity was adjusted (range from 5 to 50 V) to elicit postsynaptic potentials (PSPs) with a ~3 mV peak amplitude (Figure 1D). Following 10 min of stable baseline recording, we applied an ITDP induction protocol in CA2 that is maximally effective in CA1, consisting of 90 pairs of EC+SC stimulating pulses at a frequency of 1 Hz, at a −20 ms pairing interval (EC stimulated 20 ms before SC stimulation; Dudman et al., 2007). The paired stimuli produced a small depolarization that never reached threshold for triggering a postsynaptic CA2 action potential.

Several minutes after the ITDP pairing protocol the SC-evoked PSP started to increase in amplitude, reaching a plateau level of potentiation after 30 min of 229 ± 26% relative to baseline (n=19 neurons; Wilcoxon test, $p<0.0001$, Figure 1C–E). This is similar to the magnitude of ITDP in CA1 (PSP increased to ~250% of baseline; Basu et al., 2013; Dudman et al., 2007). In contrast to the lack of ITDP in the EC inputs to CA1 (Basu et al., 2013; Dudman et al., 2007), we observed a significant but small increase in the EC-evoked PSP to 138 ± 13% of baseline (n=17; Wilcoxon test, $p=0.002$ compared to baseline, Figure 1C–E). The large increase in the SC PSP was observed throughout the entire range of voltage stimulation intensity, with the EC PSP showing a more modest increase (Figure S1).

In CA1, ITDP is finely tuned to the −20 ms pairing interval (EC before SC), with little or no potentiation at other pairing intervals (Basu and Siegelbaum, 2015; Dudman et al., 2007). We thus tested the interval-dependence of ITDP induction in CA2 using a range of pairing delays (Figure 1F). As in CA1, the extent of CA2 ITDP was greatest at the −20 ms interval. When we reversed the pairing order, stimulating SC inputs 20 ms before EC inputs, we failed to significantly alter the SC PSP (108 ± 12 %, n=5; Wilcoxon test, $p=0.3$ compared to baseline), similar to findings in CA1 (Basu et al., 2013). However, the extent of CA2 ITDP at −10 and −30 ms intervals (145 ± 16% and 150 ± 20% respectively) was greater than typically observed in CA1 (120% and 135% respectively), indicating that CA2 ITDP is less narrowly tuned to the −20 ms interval. Nonetheless CA2 ITDP was still significantly greater using a −20 ms pairing interval compared to other intervals (Mann-Whitney test, $p=0.03$ and $p=0.04$ compared to −10 ms and −30 ms intervals respectively).

CA2 ITDP results from LTD of the IPSP through activation of δ-opioid receptors, whereas CA1 ITDP involves iLTD of cholecystokinin-positive INs

The majority of the increase in the SC-evoked PSP during ITDP in CA1 is caused by long-term depression of FFI (iLTD), resulting in a larger net depolarization (Basu and Siegelbaum, 2015). As robust iLTD in CA2 PNs can be induced by tetanic stimulation of the SC or EC inputs to CA2 (Nasrallah et al., 2015; Nasrallah et al., 2016; Piskorowski and Chevaleyre, 2013), we examined the role of iLTD in CA2 ITDP. Application of $GABA_A$ and $GABA_B$ receptor antagonist (2 μM SR 95531 and 1 μM CGP 55845, respectively) throughout the experiment fully blocked ITDP at both the SC (PSP remained at 102 ± 8 % of baseline, n=8; Wilcoxon test, p=0.9 compared to baseline) and EC inputs (PSP remained at 107 ± 23 % of baseline, n=7; Wilcoxon test, p=0.9 compared to baseline; Figure 2A and C). These results are consistent with the view that the expression of CA2 ITDP is due completely to iLTD, and differ somewhat from ITDP in CA1, where there is a residual 40% increase in the PSP in the presence of the GABA receptor antagonists as a result of long-term potentiation of SC EPSP (eLTP; Basu et al., 2013). However our results are consistent with findings that tetanic stimulation of the SC inputs fails to induce eLTP in CA2 (Dudek et al., 2016).

To confirm directly that the enhancement of the net PSP during ITDP is caused by iLTD, we recorded the feed-forward IPSC elicited by stimulation of the SC inputs in CA2 PNs under voltage-clamp conditions. We held the membrane at −10 mV to increase the outward driving force on the IPSC and reduce the EPSC driving force (Figure 2B1). The ITDP induction protocol significantly decreased the IPSC to 48 ± 11% of its initial level (n=14; Wilcoxon test, p=0.0001 compared to baseline; Figure 2B2), similar to the effects of ITDP on the IPSC seen in CA1 (Basu et al., 2013), confirming the importance of iLTD in the expression of CA2 ITDP.

Next, we examined whether the cellular and molecular mechanisms underlying ITDP in CA2 were similar to those previously described for ITDP in CA1, which results from a selective decrease in feedforward inhibition (FFI) mediated by CCK^+ basket cells through activation of CB1 receptors by endocannabinoids (Basu et al., 2013; Xu et al., 2012). However, unlike ITDP in CA1, application of the CB1R antagonist AM251 (2 μM) had no effect on the magnitude of CA2 ITDP (196 ± 16 %, n=12; Wilcoxon test, p<0.001 compared to baseline; Figure 2C).

Previous studies reported that CA2 iLTD induced by high-frequency tetanic stimulation of the SC inputs is mediated by the activation of δ-opioid receptors (Piskorowski and Chevaleyre, 2013), which suppress inhibitory synaptic transmission mediated by PV^+ INs (Svoboda et al., 1999). We found that, in CA2, a similar mechanism contributes to iLTD induced during ITDP. Using immune-histochemical labelling, we found that DORs were expressed specifically by CA2 PV^+ INs (Figure S2) in mouse hippocampus, which is somewhat different from the rat hippocampus where CA2 PNs also express DORs (Burstein et al., 2013). Bath-application of both peptide (2 μM ICI 174,864) and non-peptide (0.1 μM naltrindole) antagonists of δ-opioid receptors fully blocked ITDP (Figure 2C). Thirty minutes after delivery of the ITDP induction protocol, the SC PSP remained at 106 ± 5% of its baseline level with Naltrindole present (n=11; Wilcoxon test, p=0.2 compared to

baseline) and 102 ± 13% of baseline with ICI 174,864 (n=5; Wilcoxon test, p=0.9 compared to baseline).

Another hallmark of iLTD induced during ITDP in CA1 is that it shares certain mechanisms with eLTP, requiring activation of NMDA receptors and postsynaptic depolarization. However, blocking NMDA receptors with 50 μM D-APV had no effect on the magnitude of ITDP in CA2 (218 ± 23 %, n=11; Wilcoxon test, p=0.002 compared to baseline; Figure 2C). Additionally, chelation of intracellular Ca^{2+} by inclusion of 20 mM BAPTA in the CA2 PN patch pipette failed to inhibit CA2 ITDP (198 + 30%, n=5; Wilcoxon test, p=0.002 compared to baseline; Figure 2C), in contrast to its ability to block CA1 ITDP (Basu et al., 2013). Similarly, delivery of the ITDP induction protocol with the CA2 PN voltage-clamped at −90 mV also failed to block ITDP (210 ± 23 %, n=6; Wilcoxon test, p=0.03 compared to baseline; Figure 2C).

Although the above results show that cell-autonomous CA2 PN activity is not necessary for ITDP, it is possible that activity in neighboring CA2 PNs may provide a transcellular messenger to induce ITDP in a nearby inactivated neuron. To investigate this possibility, we inhibited the entire CA2 PN population by expressing and activating the hM4Di inhibitory DREADD receptor (iDREADD, Urban and Roth, 2015) specifically in CA2 PNs. We injected a Cre-dependent rAAV vector expressing hM4Di into the CA2 region of adult Amigo2-Cre mice, which limits Cre expression to CA2 PNs (Hitti and Siegelbaum, 2014). Although application of the specific hM4Di ligand CNO (5 μM) to hippocampal slices from mice expressing hM4Di caused a significant hyperpolarization of CA2 neurons (Fig S2C–D), it failed to reduce ITDP (224 ± 31%, n=13, Wilcoxon test, p=0.0002 compared to baseline; Figure 2C), arguing against a role for general CA2 PNs activity. Thus, although ITDP in CA1 and CA2 both involve iLTD, their cellular and molecular mechanisms differ markedly.

Expression of CA2 ITDP results from LTD of the IPSP from PV^+ INs

To explore the involvement of PV^+ INs in CA2 ITDP we examined the effect of silencing these neurons using a pharmacogenetic approach. We injected mice expressing Cre selectively in PV^+ INs (PV-Cre mice; Hippenmeyer et al., 2005) with a rAAV expressing iDREADD in a Cre-dependent manner, and performed experiments 3 weeks later in acute hippocampal slices. We observed sparse expression of iDREADD throughout the hippocampus, notably in the CA2 region around the end of the mossy fiber pathway (arrowhead in Figure 3E1). Expression of iDREADD was confined to the PV^+ INs as shown by co-labeling for iDREADD and PV (Figure 3E). Application of 5 μM CNO to hippocampal slices from mice expressing iDREADD decreased both the EC- and SC-evoked IPSCs (EC IPSC decreased by 22 ± 4 % and SC IPSC decreased by 35 ± 6 %; n=8, Wilcoxon test, p=0.008 compared to baseline in both cases; Figure S3A). As PV^+ IN-mediated inhibition accounts for approximately 50% of the total feed-forward inhibition activated by the SC pathway (Piskorowski and Chevaleyre, 2013), iDREADD activation silenced about 70% of PV-mediated FFI in these experiments.

To determine the contribution of PV^+ INs to ITDP, we examined ITDP in slices when PV^+ INs expressing iDREADD were silenced by continuous perfusion with CNO (Figure 3B1).

Although normal levels of ITDP were observed in recordings from CA2 PNs in slices from wild-type (WT) mice injected with Cre-dependent iDREADD rAAV (controls, ITDP=187 ± 16%, n=8), ITDP was largely blocked in slices from PV-Cre mice expressing iDREADD (ITDP=115 ± 13%, n=17; Mann-Whitney test, p=0.03 for control vs. PV-iDREADD; Figure 3D).

PV$^+$ INs are required for expression but not induction of ITDP

Next, we asked whether activation of the PV$^+$ IN population was required for the induction of ITDP by specifically silencing these neurons only during the 90-s pairing protocol. As CNO washout is too slow to selectively silence neurons during this 90-s period, we used an optogenetic approach We expressed YFP-tagged Archeorhodopsin 3.0 (Arch3.0-YFP; Chow et al., 2010), an inhibitory opsin, in CA2 PV$^+$ INs by injecting a Cre-dependent rAAV in the CA2 region of PV-Cre mice (Figure S4A). As with iDREADD viral injection, expression of Arch3.0-YFP was confined to PV$^+$ INs, with YFP-labeled cells and terminals prominently observed in the CA2 region defined using the PCP4 marker (Figure S3E).

Before inducing ITDP we first tested the ability of Arch3.0-YFP photo-activation to silence FFI. A 500 ms light pulse at maximum intensity caused a significant reduction in the IPSC evoked by electrical stimulation of either EC (27 ± 7% reduction, n=7; Wilcoxon test, p=0.03 compared to baseline) or SC (37 ± 3% reduction, n=15; Wilcoxon test, p=0.0002 compared to baseline; Figure S3B) inputs, indicating that Arch3.0 activation blocked about 75% of FFI mediated by the PV$^+$ INs.

Next, we applied a more prolonged period of photo-stimulation to inhibit PV$^+$ IN activity during the entire 90 s period of the ITDP pairing protocol (Figure S4B1). Despite the continuous photo-activation of Arch3.0-YFP (which silences neurons more efficiently than a brief light pulse; Chow et al., 2010), the pairing protocol still induced a large ITDP, with the SC PSP increasing to 245 ± 33% of baseline (n=13; Figure S4C), similar to that in control slices not expressing Arch3.0-YFP (PSP increased to 229 ± 26 % of baseline, n=19; Mann-Whitney test, p=0.7 control vs. Arch3.0-YFP slices, Figure S4D). Prolonged Arch3.0-mediated inhibition of the PV$^+$ INs also failed to suppress ITDP of the EC PSP. In the Arch3.0-YFP group the PSP increased to 163 ± 25% of baseline (n=7), similar to the 138 ± 13% increase in controls (n=17; Mann-Whitney test, p=0.5; Figure S4D). Therefore, we conclude that PV$^+$ INs are necessary for the *expression* of ITDP, do not need to be activated during the pairing protocol for the *induction* of ITDP.

These optogenetic experiments also provided an independent means of assessing the extent to which ITDP reduces PV-mediated FFI. Photo-activation of Arch3.0-YFP reduced the SC-evoked IPSC amplitude by 30.6 ± 3.5% before induction of ITDP but caused only an 8.9 ± 1.8% decrease in IPSC amplitude after induction of ITDP (n=12, Wilcoxon test, p=0.0002 before vs. after ITDP; Figure S3C). These results suggest that ITDP reduces the PV$^+$ IN-mediated ISPC to less than 30% of its initial level (100% × 8.9/30.7), providing provide further evidence that ITDP expression results from a decrease in PV$^+$ IN-mediated FFI.

CA2 ITDP requires paired activation of SC and EC layer II (LII) stellate cell inputs

Previous studies have shown that LII neurons in MEC and LEC send excitatory projections to CA2 PNs through SLM (Hitti and Siegelbaum, 2014; Kohara et al., 2014). As projections from other brain regions may also be present in SLM, we used optogenetic stimulation of defined EC inputs to confirm that pairing of these inputs with SC stimulation is sufficient to induce ITDP

We injected into superficial layers of medial entorhinal cortex (MEC) a rAAV vector that expressed channelrhodopsin-2 tagged with YFP under control of the CaMKII promoter (ChR2-EYFP; Figure 4A), resulting in specific expression of ChR2-EYFP in excitatory neurons in superficial MEC (Figure S5). Two weeks after the injection, we used a 1 ms light pulses to photo-stimulate the EC inputs, which evoked PSPs in CA2 PNs recorded from acute hippocampal slices (Figure 4B). After the experiment, we fixed the slices and stained for YFP, biocytin and PCP4 to confirm the expression pattern of EC fibers and the identity of the recorded cell (Figure 4E).

Pairing 1 ms light-pulse followed by electrical stimulation of the SC inputs after a 20 ms delay for 90 s at 1 Hz produced a robust ITDP of the SC-evoked PSP (Figure 4B). The peak SC-evoked depolarization measured 30 min after the pairing protocol increased to 225 ± 25% of baseline (n=11; Figure 4C), identical to that seen when ITDP was induced by paired electrical stimulation (229 ± 26 %, n=19; Mann-Whitney test, p=0.9 compared to photo-stimulation-induced ITDP; Figure 4D). The EC PSP also showed a moderate increase (130 ± 23 %, n=5; Figure 4C), also similar to that seen with paired electrical stimulation (138 ± 13 %, n=17; Mann-Whitney test, p=0.4 compared to photo-stimulation-induced ITDP; Figure 4D). Thus, we conclude that pairing of defined MEC excitatory inputs to CA2 with SC stimulation is sufficient to induce ITDP.

Direct entorhinal cortex inputs to CA2 PNs originate from LII stellate cells

Next, we sought to identify the neuronal population in EC that projects to CA2 and is responsible for the induction of ITDP. EC LII contains a mixed population of Reelin-positive stellate cells and calbindin-1-positive PNs (Kitamura et al., 2014). To determine which of these neurons project to CA2, we carried out retrograde tracing experiments by co-injecting the G-deleted SB19 strain of rabies virus (Wall et al., 2010) with Cre-dependent helper virus in the CA2 region of Amigo2-Cre mice. Ten days after injection of the GFP-expressing virus in the dorsal CA2 region of Amigo2-Cre mice (Hitti and Siegelbaum, 2014), we stained cortical slices for GFP, Reelin and calbindin-1.

We observed a preponderance of retrogradely labeled GFP-expressing cells in LII of the MEC as well as a few cells in deep layers IV and V (Figure 5B; see also Figure S6A for CA2-specificity of primary infection). Double staining for Reelin and calbindin-1 in the LEC revealed that every GFP-positive LII neuron also expressed Reelin, but not calbindin-1 (Figure 5C). Thus, we conclude that CA2 receives input from EC LII stellate cells, the same class of neurons that project to dentate gyrus and CA3. We confirmed these results using the other, more efficient, N2C strain of rabies virus (Reardon et al., 2016).

Although the above results demonstrate that, within the EC, only LII stellate cells project to CA2 PNs, it is possible that ITDP requires input from a second class of EC neurons that project to CA2 PV^+ INs. Such neurons would not be infected by the rabies virus under the above conditions. To directly confirm the importance of the LII stellate cells in ITDP, we expressed ChR2 in these neurons specifically and paired light-stimulation with electrical activation of the SC inputs. As we lack a stellate-cell specific Cre line, we used a dual viral injection strategy. We first injected a canine adenovirus 2 vector that expresses Cre (CAV2-Cre) into the dentate gyrus (DG). Two weeks later we injected a Cre-dependent ChR2-YFP virus into LEC. As CAV2-Cre travels retrogradely and is monosynaptic, it will only lead to Cre expression in neurons presynaptic to the DG (Junyent and Kremer, 2015). Given that the only EC inputs to the DG are from LII stellate cells, CAV2-Cre should be expressed specifically in these neurons in EC. To verify the efficacy of this strategy, we injected CAV2-Cre in the DG of an Ai14 reporter mouse line, which allows for TdTomato expression in neurons expressing Cre. Ten days after injection we found that nearly all TdTomato+ neurons were EC LII stellate cells and expressed the stellate marker Reelin but not the EC LII PNs marker Calbindin 1 (Figure S7).

Having verified the specificity of this approach, we repeated the CAV2-Cre injections into the DG of WT animals and two weeks later injected a Cre-dependent ChR2-YFP virus into the LEC (Figure 6A). The GFP signal was present in a pattern consistent with the expected localization to LEC LII stellate cell terminals (Kohara et al., 2014). Photo-stimulation successfully evoked an EPSP in most CA2 PNs (Figure 6B). Pairing light with SC electrical stimulation (Figure 6B1) induced a robust ITDP similar to that seen with paired electrical stimulation (Figure 6C). Thus, the SC response was increased to 208 ± 18 % of baseline (n=18) compared to 229 ± 26 % (n=19) with electrical stimulation (Mann-Whitney test, p=0.9; Figure 6D). This protocol also induced ITDP of the light-evoked EC LII stellate cell PSP (130 ± 15%, n=16, vs. 138 ± 13 %, n=17 for electrical stimulation; Mann-Whitney test, p=0.7; Figure 6D).

As discussed above, CA2 ITDP does not appear to require postsynaptic depolarization of the CA2 PN during the pairing protocol. We were able to specifically demonstrate that the presence of an EC-evoked PSP in CA2 PNs is not required for the induction of ITDP by examining a subset of recordings in which photo-stimulation of the EC inputs failed to evoke a noticeable depolarizing PSP in the patch-clamped CA2 PN, although there was strong expression of ChR2-GFP in fibers extending to CA2 in the same slice (same pattern as in Figure 6E1). The absence of a photo-stimulated PSP was not a result of our having severed the distal dendrites during slice preparation as the same CA2 PNs displayed a normal-sized EC PSP with distal electrical stimulation but likely reflects heterogeneity in innervation of individual CA2 PNs by ChR2-expressing axons from EC. Surprisingly, the pairing protocol induced a large ITDP in the electrically evoked SC PSP in the same CA2 PNs that failed to generate an EPSP in response to EC photo-stimulation (PSP increased to 230 ± 23% of baseline, n=6 for photo-stimulation vs. 229 ± 26 %, n=19 for electrical stimulation; Mann-Whitney test, p=0.6; Figure 6D). We also saw a normal-sized ITDP in the electrically evoked EC PSP (151 ± 21% for ITDP from non-photoresponsive cells, n=5, vs. 138 ± 13% for ITDP induced electrically, n=17; Mann-Whitney test, p=0.5; Figure 6D). These results extend our

findings that the induction of ITDP does not require that the CA2 PN itself be activated during the ITDP pairing protocol (Figure 2C).

Sites of enkephalin release in CA2

What is the site of enkephalin release required for the induction of CA2 iLTD and ITDP? Interestingly, enkephalins have been detected in INs that synapse onto other INs (Blasco-Ibanez et al., 1998; Commons and Milner, 1996), including those synapsing onto PV^+ basket-cell INs (Fuentealba et al., 2008). We screened a number of enkephalin antibodies and identified two that provided a consistent pattern of staining. Enkephalin was found in a number of presynaptic terminals and pathways that impinged on CA2, including mossy fiber inputs to CA3 and CA2 from dentate gyrus granule cells (arrowhead in Figure 7A), as previously reported (Chavkin et al., 1983; Chavkin et al., 1985; Gall et al., 1981; McGinty et al., 1983; Terrian et al., 1988). We also observed staining surrounding CA2 PN soma (Duka et al., 1981). Double labeling for enkephalin and PV also revealed prominent staining for enkephalin surrounding PV^+ IN soma located in or near the CA2 PN cell body layer (Figure 7B and 7C). Although these results indicate the presence of enkephalin-positive (ENK^+) neurons in the CA2 region, the specific neuronal population that releases enkephalin for the induction of ITDP remains unknown.

Blockade of δ-opioid receptors within CA2 inhibits social memory behavior

What functional role might CA2 ITDP, or its underlying plasticity mechanism of iLTD, play in hippocampal dependent learning and memory? Previous studies have implicated CA2 in social memory (Hitti and Siegelbaum, 2014; Stevenson and Caldwell, 2014), whereas ITDP in CA1 has been proposed to enhance the specificity and strength of contextual and object memory (Basu et al., 2016). As activation of DORs is required for both ITDP (Figure 2C) and iLTD (Piskorowski and Chevaleyre, 2013), we explored the effect on social memory of infusion of a specific DOR antagonist through a cannula targeting CA2. Although drug infusion lacks the specificity of genetic inactivation, long-lasting effects of bath application of the DOR-selective agonist DPDPE to hippocampal slices are restricted to CA2 as the DOR agonist DPDPE selectively induces iLTD of PV^+ IN-mediated FFI in CA2 PNs (Piskorowski and Chevaleyre, 2013), while causing only a transient inhibition of FFI in neighboring CA1 neurons (Piskorowski and Chevaleyre, 2013). Moreover, we found that DOR activation had no effect on inhibition or excitation in CA3 (Figure S8A). As DOR signaling appears to have a selective long-lasting action in CA2 but not in surrounding CA1 or CA3 regions, any behavioral effects of *in vivo* infusion of a DOR antagonist into the CA2 region likely results from its actions in CA2.

We implanted 3-month-old WT animals with bilateral cannulas and perfused 1 μl of the DOR antagonist naltrindole (5 mM solution) 30 min before performing the direct interaction test of social memory (Figure 8A; Kogan et al., 2000). In this test, the subject mouse is allowed to interact with a novel juvenile mouse for two 2-min trials separated by a 30 min inter-trial interval (Figure 8A). Social memory is evidenced by the lower interaction time in trial 2 compared to trial 1. In saline infused control animals, the average interaction time was 58 ± 5 s during the first trial and decreased to 24 ± 4 s during the second trial, indicative of social memory (n=9; Wilcoxon test, p=0.004 compared to baseline; Figure 8B and

Supplementary video 1). Although naltrindole-infused animals also showed a decreased interaction time from trial 1 (52 ± 4 s) to trial 2 (36 ± 5 s; n=9; Wilcoxon test, p=0.01 compared to baseline; Figure 8B and Supplementary video 2), the percent reduction in the drug-treated group (31 ± 8%, n=9) was significantly smaller than the reduction in the control group (60 ± 7%, n=9; Mann-Whitney test, p=0.008; Figure 8C). After the experiment, we perfused each animal with 1 μl of the dye mini-Ruby (5 mM solution) to verify the location of the perfusion. Most of the dye was co-labeled with the CA2 marker RGS14, with a moderate extent of dye leakage in CA3a or CA1c regions adjacent to CA2 that do not show long-term DOR actions.

Social interactions that engage social memory occlude ITDP and reduce FFI

Next, we asked whether social interactions with a novel animal that lead to social memory storage may recruit ITDP (or a related plasticity process). To explore this possibility, we performed an occlusion experiment to determine whether exposure of an adult male subject mouse to a novel juvenile mouse for 2 min altered the magnitude of ITDP in slices prepared from the subject mouse within 45 min of the interaction. The amount of potentiation of the SC PSP following induction of ITDP was significantly reduced in slices obtained from mice that received a novel social stimulus (PSP was increased to 122 ± 6% of baseline, n=9) compared to slices obtained from mice exposed to a littermate for 2 min (PSP was increased to 229 ± 26 % of baseline, n=19; Mann-Whitney test, p=0.0007; Figure 8E). The reduction in ITDP after a novel social interaction is consistent with the idea that this interaction is sufficient to recruit ITDP, thereby occluding further potentiation in the slice recordings.

If social interaction between a subject mouse and a novel animal does indeed recruit ITDP or a related plasticity process that recruits iLTD, then the amount of FFI should also be reduced in slices obtained from the subject mouse. To explore this possibility, we compared the size of the IPSC recorded from CA2 neurons in response to SC stimulation in slices obtained from mice exposed to a novel animal for 2 min (experimental group) compared to slices from control mice exposed to a littermate for 2 min (3 mice and 10 cells for each condition). The amount of FFI recorded in CA2 PNs was indeed significantly smaller in slices prepared from the experimental group compared to slices from the control group (ANOVA novelty factor $F\{1,237\}=50.72$, $p<0.0001$, Figure S8B). Thus, both our behavioral and slice electrophysiology experiments support the idea that DORs in CA2 regulate the strength of social memory through induction of ITDP or a closely related mechanism.

Discussion

We report that CA2 PNs exhibit a robust increase in the magnitude of the peak depolarization of the SC-evoked PSP in response to paired activation of their EC and SC inputs. In many respects, this plasticity is similar to ITDP in CA1 (Dudman et al., 2007). Similar to CA1 ITDP, CA2 ITDP was induced by low-frequency, subthreshold pairing of EC and SC inputs that failed to elicit CA2 action potentials. Moreover, ITDP in CA2 was maximal when the SC inputs were activated 20 ms after the EC inputs, similar to the timing-dependence of ITDP in CA1. Finally, as in CA1 (Basu et al., 2013), the increase in the net PSP in CA2 depends on LTD of feedforward inhibition (iLTD).

However, in a number of other respects ITDP in CA2 differs from that in CA1. Whereas ITDP in CA1 is driven by EC layer III (LIII) PN projections to CA1 distal dendrites, ITDP in CA2 requires input from EC LII stellate cells. CA1 and CA2 ITDP also differ in their molecular mechanisms. Thus, ITDP and iLTD in CA2 requires activation of δ-opioid receptors, which selectively regulate FFI mediated by PV^+ INs. In contrast, ITDP in CA1 depends on activation of endocannabinoid CB1 receptors, which suppress inhibition mediated by CCK^+ INs. In addition, whereas CA1 ITDP requires postsynaptic depolarization, NMDA receptor activation and dendritic integration of the EC and SC inputs by the CA1 PN (Basu et al., 2016), CA2 ITDP does not require CA2 PN depolarization or NMDA receptor activation. This suggests that the site of integration of CA2 ITDP lies outside of the CA2 PN. Finally, ITDP is more precisely tuned to the 20 ms pairing interval in CA1 compared to CA2. This may reflect the differential contribution of long-range inhibitory projections from EC, which enable CA1 ITDP induction by suppressing a population of dendrite-targeting CA1 INs. These inputs do not project to CA2 (Basu et al., 2016).

The differential role of δ-opioid receptor-dependent inhibition of PV^+ INs CA2 ITDP

The mechanism underlying ITDP in CA2 resembles δ-opioid receptor-dependent iLTD induced by unpaired high-frequency tetanic stimulation of CA2 SC inputs (Nasrallah et al., 2015; Piskorowski and Chevaleyre, 2013) or EC inputs (Nasrallah et al., 2016). Similarly, the mechanism underlying the iLTD component of ITDP in CA1 (Basu et al., 2013) resembles CB1R-dependent iLTD induced by high-frequency tetanic stimulation of the CA1 SC inputs (Chevaleyre and Castillo, 2004). Thus, in both CA1 and CA2, paired low-frequency activation of the EC and SC inputs recruit similar forms of plasticity induced by high frequency stimulation of the SC inputs alone, even though the class of inhibitory neurons mediating the plasticity in these two regions differ. This raises the interesting question as to why distinct IN populations contribute to iLTD and ITDP in neighboring hippocampal regions.

The involvement of PV^+ INs in CA2 ITDP is consistent with findings that this region contains a higher density of PV^+ INs compared to neighboring CA1 and CA3, both in mice (Piskorowski et al., 2016) and humans (Andrioli et al., 2007; Benes et al., 1998). Light-induced stimulation of the PV^+ INs elicited larger IPSCs on CA2 PNs than on CA1 PNs (Piskorowski and Chevaleyre, 2013). Additionally, some PV^+ cells in CA2 have a unique morphology and extend their dendrites and axons into the three CA subfields (Mercer et al., 2012; Mercer et al., 2007). Finally CA2 PNs receive a much higher density of inhibitory synapses from PV^+ INs cells compared with CA1 or CA3 (Ribak et al., 1993). These observations are consistent with the higher feedforward inhibition on CA2 PNs evoked by SC stimulation (Chevaleyre and Siegelbaum, 2010).

However, PV^+ IN density alone is unlikely to account for all the differences in iLTD in CA1 compared to CA2. Thus, whereas bath-application of a δ-opioid receptor agonist is sufficient to produce a long-lasting suppression of PV^+ IN-mediated inhibition in CA2, it produces only a transient suppression of inhibition in CA1 (Piskorowski and Chevaleyre, 2013). This difference may be related to differences in δ-opioid receptor density, as radiolabeling of

DORs was largely confined to CA2 (Duka et al., 1981), even though DOR mRNA expression is detected throughout the SLM of the hippocampus (Erbs et al., 2012; Stumm et al., 2004).

The site of EC and SC input integration and the triggering of enkephalin release for the induction of CA2 ITDP

The differential role of δ-opioid receptor dependent plasticity in CA2 vs. CA1 is also likely to depend on local differences in the release of enkephalin, the endogenous agonist for the δ-opioid receptor, as strong enkephalin radiolabeling is localized to CA2 (Sar et al., 1978). This may reflect the fact that, in the hippocampus, one site of enkephalin release is from mossy fiber terminals, which target CA2 but not CA1 (Kohara et al., 2014). Moreover, enkephalin is also present in LEC LII stellate cells, which target CA2 but not CA1, as well as in a sparse population of INs distributed across the different hippocampal layers (Gall et al., 1981; Simmons and Chavkin, 1996).

Despite the striking similarities between our results on CA2 ITDP and the mechanisms of iLTD, it is unclear as to whether the two protocols release enkephalin from the same cells. As 1 Hz stimulation of SC or EC inputs alone fails to elicit iLTD (97 ± 9 %, n=5; Wilcoxon test, p=0.1 compared to baseline for EC stimulation; see Piskorowski and Chevaleyre (2013) for SC 1 Hz stimulation), enkephalin release appears to require strong synaptic activation, either through paired stimulation of EC and SC pathways, which occurs during ITDP induction, or through higher frequency unpaired SC (Piskorowski and Chevaleyre, 2013) or EC (Nasrallah et al., 2016) stimulation. Indeed neuropeptide release generally requires higher levels of presynaptic activity than does release of classical neurotransmitters (van den Pol, 2012).

What is the site of integration of the EC and SC inputs during the induction of ITDP? In CA1, this integration occurs in CA1 PNs as their hyperpolarization or intracellular perfusion with a Ca^{2+} chelator, blocks the induction of ITDP. However, the integration of EC and SC signals during CA2 ITDP is likely to occur in a non-pyramidal neuronal or glial cell within the hippocampus because hyperpolarization of the CA2 PN population fails to inhibit ITDP. We suggest that EC and SC inputs may converge on enkephalin-expressing INs in or nearby to CA2, synergistically triggering enkephalin release.

This leads to the proposed circuit mechanism for CA2 ITDP (Figure S9). According to this model, enkephalin expressing neurons integrate appropriately timed EC LII stellate cell and SC inputs to generate a large postsynaptic response required to release enkephalin. The large postsynaptic response can also be elicited by strong tetanic stimulation of either pathway alone, explaining the observed induction of iLTD with unpaired strong EC or SC activation (Nasrallah et al., 2015, 2016; Piskorowski and Chevaleyre, 2013). As we observed ENK^+ terminals apposed to CA2 PNs and PV soma (Figure 7), enkephalin could be released directly onto PV^+ basket cell terminals to produce a long-lasting presynaptic inhibition of GABA release.

Physiological relevance of ITDP in CA2 compared to CA1

Heterosynaptic learning rules have been posited to act as salience detectors (Basu and Siegelbaum, 2015). ITDP in CA1 has been suggested to provide a mechanism that assesses the relevance of information propagated through the trisynaptic pathway based on its temporal relation to multimodal sensory representations arriving through the direct EC inputs (Basu et al., 2013; Basu et al., 2016; Dudman et al., 2007). Others have shown that paired activation of EC and SC inputs to CA1 can produce shorter-term actions to boost CA1 output by promoting EPSP dendritic propagation (Jarsky et al., 2005) or burst firing of action potentials (Takahashi and Magee, 2009). A potential behavioral role of CA1 ITDP, or a related plasticity mechanism, was recently suggested by a study from our laboratory in which the long-range inhibitory inputs from EC to CA1 were inactivated using a pharmacogenetic approach (Basu et al., 2016). Silencing the long-range inhibitory inputs prevents the induction of CA1 ITDP results in a decrease in specificity of contextual fear memory and reduced performance in a novel object recognition memory test. In a similar manner, we find that a plasticity mechanism related to CA2 ITDP and/or iLTD may also be required for optimal CA2-dependent memory performance as the infusion of the DOR antagonist naltrindole in CA2 reduced performance on a social memory task. As the DOR antagonist blocks both iLTD and ITDP, we cannot determine whether the impairment in social memory results from a loss of ITDP, iLTD or some other DOR-dependent mechanism that targets inhibition. However, our finding that social interaction with a novel animal is sufficient to reduce FFI and occlude further induction of ITDP in acute hippocampal slices is consistent with the view that ITDP or iLTD are engaged during social memory storage.

The finding that CA2 ITDP can be induced with much weaker, lower-frequency stimulation compared to CA2 iLTD suggests that ITDP is likely to be recruited preferentially under physiological conditions of sparse firing patterns observed *in* vivo such as the 1Hz EC-hippocampal firing frequency observed in rodents during exploratory behavior (Csicsvari et al., 1999; Frank et al., 2001). The 20 ms timing-dependence of ITDP also suggests a potential physiological relevance as this delay matches the delay in which information is propagated through the trisynaptic vs. direct EC inputs during electrical stimulation in vivo (Yeckel and Berger, 1990), and matches the period of network-dependent gamma frequency oscillations. However, little is known about the *in vivo* dynamics of CA2 EC and SC inputs during social interactions or other behaviors. Thus future *in vivo* monitoring of EC and SC inputs to CA2 during social memory storage, although challenging, would help assess the potential relevance of ITDP under more physiological conditions.

What are the relative roles of the direct EC vs. SC inputs to CA2 in social memory? As CA2 PNs are weakly excited by their SC inputs (as a result of strong FFI) but are strongly excited by their direct EC inputs (Chevaleyre and Siegelbaum, 2010), the SC inputs were proposed to primarily act in CA2 to prevent information flow through a quadrisynaptic path (EC→DG→CA3→CA2→CA1). Our findings implicating ITDP and/or iLTD of SC-evoked feedforward inhibition to CA2 in social memory suggest that the SC inputs may provide important information for social memory storage. These observations complement the findings of a previous study linking the potentiation of the SC-evoked EPSP in CA2 PNs by vasopressin (Pagani et al., 2015) to a vasopressin-dependent enhancement in social memory

(Smith et al., 2016). Thus, optimal social memory storage may require both the DOR-mediated depression of SC-evoked FFI and the vasopressin-mediated potentiation of the SC-evoked EPSP in CA2 PNs. The potentiation of the SC EPSP by vasopressin could account for the residual social memory we observed in the presence of the DOR antagonist.

Our results on the importance of PV^+ INs in CA2 social memory storage add to the growing literature on the importance of these neurons and different plasticity mechanisms in different forms of hippocampal-dependent learning and memory. Thus, hippocampal PV^+ INS have recently been linked with memory consolidation following single-trial contextual fear conditioning (Ognjanovski et al., 2017) as well as environmental enrichment and Pavlovian contextual fear conditioning (Donato et al., 2013). Moreover, environmental enrichment and Pavlovian contextual fear conditioning triggered the differentiation of the PV^+ INs network into low-expressing or high-expressing PV^+ network configurations, respectively (Donato et al., 2013). The low-PV^+ configuration was associated with enhanced structural synaptic plasticity and memory consolidation and retrieval, which were reduced in the high-PV configuration. Whether other forms of PV^+ neuron plasticity also contribute to social memory storage in CA2 in addition to ITDP/iLTD remains to be determined.

Finally, recent findings that ventral CA1 is also required for social memory (Okuyama et al., 2016) suggest that plasticity in CA2 may ultimately be expressed by enhanced activation of downstream CA1 PNs. Although further studies will be important to dissect the relative contributions of different circuit elements and plasticity mechanisms to social memory storage, our results, together with previous findings from our lab on CA1 ITDP (Basu et al., 2016), suggest that enhancement of information flow through the SC pathway through ITDP may provide a widespread synaptic learning rule that is tuned to the local regional molecular and cellular circuitry and which may serve to enhance performance in diverse hippocampal-dependent memory tasks.

STAR METHODS

CONTACT FOR REAGENT AND RESOURCE SHARING

Further information and requests for reagents may be directed to, and will be fulfilled by the Lead Contact, Dr. Steven A. Siegelbaum (sas8@columbia.edu).

EXPERIMENTAL MODEL AND SUBJECT DETAILS

All animal procedures were performed in accordance with the regulations of the Columbia University IACUC. 6- to 12-week-old C57BL6/J male mice were used in this study for most electrophysiological and labelling studies. When required, we also used males of the same age range from the following transgenic mouse lines PV-Cre mice (Jackson Laboratories #017320), Ai14 mice (Jackson Laboratories #007914) and Amigo2-cre (Jackson Laboratories #030215). Noteworthy, all transgenic mice used in this study were kept on a C57BL6/J strain background.

METHOD DETAILS

Slice preparation—We prepared transverse hippocampal slices from 8- to 12-week-old C57BL6 male mice. Animals were killed under isoflurane anesthesia by perfusion into the right ventricle of ice-cold solution containing the following (in mM): 10 NaCl, 195 sucrose, 2.5 KCl, 10 glucose, 25 $NaHCO_3$, 1.25 NaH_2PO_4, 7 Na Pyruvate, 1.25 $CaCl_2$, and 0.5 $MgCl_2$. Hippocampi were dissected from the brain in the same dissecting solution, placed upright into a 4% agar mold, and cut into 400 μm slices with a vibratome (VT1200S, Leica) in the same ice-cold dissection solution. Slices were then transferred to a chamber containing 50% dissecting solution and 50% ACSF (in mM: 125 NaCl, 2.5 KCl, 22.5 glucose, 25 $NaHCO_3$, 1.25 NaH_2PO_4, 3 Na Pyruvate, 1 Ascorbic acid, 2 CaCl2 and 1 MgCl2). The chamber was kept at 34°C for 30 min and then at room temperature for at least 1 h before recording. All experiments were performed at 33°C. Dissecting and recording solutions were both saturated with 95% O2 and 5% CO2, pH 7.4.

Electrophysiological recordings—Slices were mounted in the recording chamber under a microscope. Recordings were acquired using the Multiclamp 700A amplifier (Molecular Device), data acquisition interface ITC-18 (Instrutech) and the Axograph X software.

We targeted CA2 PNs based somatic location and size in both deep and superficial layer. Whole-cell recordings were obtained from CA2 PNs in current-clamp mode held at −73 mV with a patch pipette (3–5 MΩ) containing the following (in mM): 135 K methylsulfate, 5 KCl, 0.2 EGTA-Na, 10 HEPES, 2 NaCl, 5 ATP, 0.4 GTP, 10 phosphocreatine, and 5 μM biocytin, pH 7.2 (280–290 mOsm). The liquid junction potential was 1.2 mV and was left uncorrected. Inhibitory currents were recorded with pipette solution containing 135 Cs methylsulfate instead of K methylsulfate. Series resistance (15–25 MΩ) was monitored throughout each experiment; cells with a >20% change in series resistance were discarded. Once whole-cell recording was achieved we confirmed the cell-type based on the following electrophysiological properties: input resistance (60 to 120 MΩ), resting membrane potential (below −70 mV), sag amplitude (smaller than 5 mV) and presence of a slow depolarization prior discharge upon the injection of a long current pulse (Figure 1A1).

For electrical stimulation, synaptic potentials from the Schaffer collateral (SC) and direct entorhinal cortex fibers (EC) were evoked by monopolar stimulation with pipettes filled with 1-M NaCl and positioned in the *stratum radiatum* (*SR*) of CA3 (SC stimulation) as well as in the *stratum lacunosum-moleculare* (*SLM*) of CA1a, near the hippocampal fissure (EC stimulation, Figure 1B1). The ITDP induction protocol (90 paired pulses at 1 Hz with EC stimulation 20 ms prior to the SC stimulation, (Dudman et al., 2007) was applied after a stable baseline of 5 min at least 10 min following breaking into the cell.

For light stimulation, pulses of blue or yellow light (pE-100, Cool LED) were delivered through a 40× immersion objective and illuminated an area of 0.2 mm^2. The illumination field was centered over the CA2 pyramidal cell layer for yellow light illumination and over the SLM layer for blue light illumination.

In a subset of experiments, the following drugs were used at the following concentrations via bath application (unless otherwise noted): SR95531 (2 mM, Tocris #1262), CGP55845 (1 mM, Tocris #1248), AM251 (2 mM, Tocris #1117), D-APV (100 mM, Tocris #0106), ICI 174,864 (2 μM, Tocris #0820), BAPTA (20 mM, Tocris #2786) and naltrindole (0.1 μM, Sigma-Aldrich #N115).

Virus injections—For all injections, animals were anesthetized using isoflurane and given analgesics. A craniotomy was performed above the target region and a glass pipette was stereotaxically lowered down the desired depth. Injections were performed using a nano-inject II (Drummond Scientific company). 23 nL was delivered 15 s apart until total amount was reached. The pipette was retracted after 5 min.

iDREADD and Arch3.0 hippocampal injections: We injected bilaterally 200 nL of either rAAV2 hsyn.DIO.HA-hM4D(Gi).IRES.mCitrine (Addgene #50455 prepared by the UNC vector core) or rAAV9 CBA.FLEX.Arch3.0-GFP.WPRE.SV40 (U Penn, AV-5-PV2432, lot V42-43MI-S, prepared from Addgene #22222) into the hippocampi of PV-Cre mice (Jackson Laboratories #017320) or Amigo2-cre mice (Jackson Laboratories #030215). Injection coordinates were the following (in mm from Bregma): AP 1.6, ML ±1.6, DV 1.7. Acute slices were prepared 3 weeks after the injection.

Rabies tracing: We stereotaxically delivered 50 nl of a 1:2 cocktail of rAAV5 EF1a.FLEX.TVA-mCherry (Addgene #38044 prepared by UNC vector core) with rAAV5 CAG.FLEX.RAB[G] (Addgene #48333 prepared by UNC vector core) into the dorsal hippocampus of Amigo2-cre mouse (Hitti and Siegelbaum, 2014): AP 1.6, ML ±1.6, DV 1.7 (in mm from Bregma). Following 2 weeks of recovery and rAAV expression, a secondary surgery was performed by the same technique and 300 nl of RABV$^{\Delta G}$-eGFP[EnvA] (SAD-B19 strain, Addgene #32636 prepared by the Salk institute vector core) was injected at the same coordinates. Mice were killed 7 d later and the brains cut sagittally for EC imaging or coronally for HC imaging. We repeated these experiments using 50 nL of the helper viruses rAAV5 EF1a.FLEX.TVA-mCherry mixed with rAAV-FLEX-nGFP-2A-G (histone2B-GFP fusion: nGFP, Addgene # 73476, (Reardon et al., 2016) and followed by 300 nL of the rabies virus RABV$^{\Delta G}$–mCherry[EnvA] (CVS-N2c strain, Addgene #73464, (Reardon et al., 2016).

Channel rhodopsin expression into the MEC: We injected 200 nL rAAV9 CaMKIIa.hChR2(H134R)-EYFP (Addgene #26969 prepared by UNC vector core) into the MEC at the following coordinates: AP −4.7, ML ±3.35 and DV −3.3 (in mm from Bregma). Animals were processed for acute slice physiology 10–15 days after. Because of the extensive overlapping of GFP^{+} fibers in the EC we used a similar virus expressing cell-filling diffusible mCherry to check for the specificity of the expression. To label the somas, we injected 200 nL of rAAV9 CamKII.hChR2(T/C).p2A.mCherry (prepared by Stanford vector core) at the same coordinates and perfused the mice after 15 days.

Dual viral injections to target the EC LII stellate cells: We injected bilaterally 50 nL of CAV2-Cre virus (molecular genetic institute of Montpellier viral vector core, (Junyent and Kremer, 2015) into the DG of Ai14 mice (Jackson Laboratories #007914). Animals were perfused 10 days later and sagittal slices were prepared to visualize the LEC. We repeated

these injections on WT animals followed 10 days later by the bilateral injection of 200 nL rAAV5 EF1a.DIO.hChR2(E123T/T159C).eYFP (Addgene #35509 prepared by the UNC vector core, lot AV4828b) into the LEC. Acute slices were prepared from the animals 10–15 days later.

Immunohistochemistry (IHC)—For staining following rabies injections, the animals were intra-cardiacally perfused using saline then 4% PFA in PBS. The brains were quickly extracted and incubated in 4% PFA overnight. After 1 h washing in 0.3% glycine in PBS, 60 μm slices were prepared (Leica VT1000S). After fixation, slices were permeabilised and blocked for 2h with 5% goat-serum and 0.5% Triton-X in PBS. Slices were incubated overnight with primary antibodies at 4°C diluted in 5% goat-serum and 0.1% Triton-X in PBS. The slices were washed 3 times 15 min in PBS and secondary antibodies were applied at room temperature for 2 h at a concentration of 1:500 in in 5% goat-serum and 0.2% Triton-X in PBS. For *post hoc* immunocytochemistry after patch-clamp recordings, slices were fixed for 1 h in 4% PFA in PBS and streptavidin-Alexa 555 (1:500, Thermo Fisher Scientific, Cat# s21381) was applied during primary and secondary incubations. All secondary antibodies were produced in the goat. DAPI staining was performed (Hoechst 33342 at 1:1000 for 5 min in PBS at RT) prior to mounting the slice using fluoromount (Sigma-Aldricht). Images were acquired using an inverted confocal microscope (Leica LSM 700).

For STEP and biocytin staining, first incubation was performed with primary antibody mouse isotype1 antibody to STEP (1:500, Cell Signaling Technology, Cat# 4396S) as well as streptavidin conjugated to Alexa 555 (1:500, Thermo Fisher Scientific, Cat# s21381). Secondary incubation was performed in the presence of the antibody to mouse isotype 1 conjugated to Alexa 488 (1:500, 1:500, Thermo Fisher Scientific, Cat# A21121) as well as streptavidin conjugated to Alexa 555 (1:500, Thermo Fisher Scientific, Cat# s21381).

For DOR and PV staining, first incubation was performed with a mouse antibody to PV (1:4000, Sigma-Aldrich, Cat# P3088) and rabbit antibody to DOR (1:250, EMD Millipore, Cat# AB1560). They were followed by the secondary antibody to rabbit conjugated to Alexa 488 (1:500, Thermo Fisher Scientific, Cat# A11008) and the secondary antibody to mouse IgG1 conjugated to Alexa 633 (1:500, Thermo Fisher Scientific, Cat# A21126).

For mCitrine and RGS 14 staining, first incubation was performed with a chicken antibody to GFP (1:1000, AVES Labs, Cat# GFP-1020) and mouse antibody to RGS14 (1:50, UC Davis/NIH NeuroMab Facility, Cat# 73–170). They were followed by the secondary antibody to chicken conjugated to Alexa 488 (1:500, Thermo Fisher Scientific, Cat# A11039) and the secondary antibody to mouse IgG2a conjugated to Alexa 647 (1:500, Thermo Fisher Scientific, Cat# A21241).

For Parvalbumin and mCitrine staining, first incubation was performed with the following primary antibodies: rabbit antibody to parvalbumin (1:500, Abcam, Cat# ab11427) and chicken antibody to GFP (1:1000, AVES Labs, Cat# GFP-1020). Secondary incubation was performed with the following: antibody to rabbit conjugated to Alexa 633 (1:500, Thermo

Fisher Scientific, Cat# A21070) and antibody to chicken conjugated to Alexa 488 (1:500, Thermo Fisher Scientific, Cat# A11039).

For mCitrine and biocytin staining, first incubation was performed with the following: chicken antibody to GFP (1:1000, AVES Labs, Cat# GFP-1020) and streptavidin conjugated to Alexa 555 (1:500, Thermo Fisher Scientific, Cat# s21381). Secondary incubation was performed with the following: antibody to chicken conjugated to Alexa 488 (1:500, Thermo Fisher Scientific, Cat# A11039) and streptavidin conjugated to Alexa 555 (1:500, Thermo Fisher Scientific, Cat# s21381).

For YFP, biocytin and PCP4 staining, first incubation was performed with the following: chicken antibody anti-GFP (1:1000, AVES Labs, Cat# GFP-1020), rabbit antibody to PCP4 (1:200, Sigma-Aldrich, Cat#; HPA005792) and streptavidin conjugated to Alexa 555 (1:500, Thermo Fisher Scientific, Cat# s21381). Secondary incubation was performed with the following: antibody to chicken conjugated to Alexa 488 (1:500, Thermo Fisher Scientific, Cat# A11039), streptavidin conjugated to Alexa 555 (1:500, Thermo Fisher Scientific, Cat# s21381) and antibody to rabbit conjugated to Alexa 633 (1:500, Thermo Fisher Scientific, Cat# A21070).

For YFP, reelin and calbindin 1 staining, first incubation was performed with the following: chicken antibody to GFP (1:1000, AVES Labs, Cat# GFP-1020), mouse antibody to reelin (1:250, MBL International, Cat# D223-3) and rabbit antibody to calbindin1 (1:1000, Abcam, Cat# ab11426). Secondary incubation was performed with the following: antibody to chicken conjugated to Alexa 488 (1:500, Thermo Fisher Scientific, Cat# A11039), antibody to mouse IgG1 conjugated to Alexa 546 (1:250, Thermo Fisher Scientific, Cat# A21123) and antibody to rabbit conjugated to Alexa 633 (1:500, Thermo Fisher Scientific, Cat# A21070).

For YFP, biocytin and RGS14 staining, first incubation was performed with the following: chicken antibody to GFP (1:1000, AVES Labs, Cat# GFP-1020), streptavidin conjugated to Alexa 555 (1:500, S21381, Thermo Fisher) and mouse IgG2a antibody to RGS14 (1:50, UC Davis/NIH NeuroMab Facility, Cat# 73–170). Secondary incubation was performed with the following: antibody to chicken conjugated to Alexa 488 (1:500, Thermo Fisher Scientific, Cat# A11039), streptavidin conjugated to Alexa 555 (1:500, Thermo Fisher Scientific, Cat# s21381) and antibody to mouse IgG2a conjugated to Alexa 647 (1:500, Thermo Fisher Scientific, Cat# A21241).

For enkephalin and parvalbumin staining, first incubation was performed with the following: mouse antibody to enkephalin (1:50, Fitzgerald Industries International, Cat# 10-L20A; Figure 7A,B or 1:50, Santa Cruz Biotechnologies, Cat# sc-47705; Figure 7C) as well as rabbit antibody to parvalbumin (1:500, Abcam, Cat# ab11427). Secondary incubation was performed with the following: antibody to mouse conjugated to Alexa 488 (1:500, Thermo Fisher Scientific, Cat# A11001) and antibody to rabbit conjugated to Alexa 633 (1:500, Thermo Fisher Scientific, Cat# A21070).

For TdTomato, CaMKII and GAD67 staining, first incubation was performed with the following: mouse antibody to GAD67 (1:1000, Millipore, Cat# MAB5406) and rabbit

antibody to CaMKII (1:200, Abcam, Cat# ab22609). We did not stain for TdTomato since the endogenous fluorescent signal was bright enough. Secondary incubation was performed with the following: antibody to mouse IgG2a conjugated to Alexa 488 (1:500, Thermo Fisher Scientific, Cat# A21131) and antibody to rabbit conjugated to Alexa 633 (1:500, Thermo Fisher Scientific, Cat# A21070).

For TdTomato, reelin and calbindin1 staining, first incubation was performed with the following: mouse antibody to reelin (1:250, MBL International, Cat# D223-3) and rabbit antibody to calbindin 1 (1:1000, Abcam, Cat# ab11426). We did not stain for TdTomato since the endogenous fluorescent signal was bright enough. Secondary incubation was performed with the following: antibody to mouse IgG1 conjugated to Alexa 633 (1:500, Thermo Fisher Scientific, Cat# A21126) and antibody to rabbit conjugated to Alexa 488 (1:500, Thermo Fisher Scientific, Cat# A11008).

For mCherry and reelin staining, first incubation was performed with a mouse antibody to reelin (1:250, MBL International, Cat# D223-3) followed by the secondary antibody to mouse IgG1 conjugated to Alexa 633 (1:500, Thermo Fisher Scientific, Cat# A21126). We did not stain for mCherry since the endogenous fluorescent signal was bright enough.

Direct interaction test—For social recognition experiments we used 3-month-old grouped house mice (5 per cages). Mice were implanted with a cannula guide extending for 1.5 mm (C315G 2-G11-SPC, Plastics One). The scalp was removed and scored before holes were drilled (AP −2 mm; ML ±3 mm from Bregma). Cannula guides were implanted bilaterally at a 10° angle and kept in place using glue. The skull was then covered with dental cement (GC FujiCEM 2) and dummy cannulas (C315DC-SPC, Plastics One) were inserted into the guides. Mice were returned to their home cage and left to recover for 1 week at least.

For the direct interaction test we used the procedure described by Kogan et al. (2000) adapted to accommodate the micro-infusion. The procedure was performed shortly after the beginning of the dark cycle. Mice were placed under a light isoflurane anesthesia (2%) and the dummy cannulas were removed. We inserted cannulas projecting 0.5 mm from the cannula guide (C315I-SPC, Plastics One) and screwed onto the guides. 1 μL of 5 μM naltrindole diluted in 0.9% saline or 1 μL of 0.9% saline was injected on each side over 10 min using a syringe pusher (Fusion 200, Chemix Inc.) mounted with two 2 μL syringes (88511, Hamilton). Cannulas were removed 2 min after the end of the micro-infusion to avoid pulling out the drug when removing the cannulas. Mice typically recovered fully from the light anesthesia within 5 min.

At the end of the infusion, mice were single-housed into plastic boxes of dimensions similar to their home cage (length 13" length × 7–1/2" width) but taller (8–1/4" height) to allow filming the interactions from the top (see supplementary videos) while preventing them from escaping. Boxes contained fresh litter. Mice were left to habituate for 30 min in the behavioral room under dim light conditions. A grouped-housed male juvenile mouse (4 weeks old) was then placed in each box for a first interaction trial of 2 min. Following a 30

min inter-trial delay, the same juvenile was placed into the adult's cage for a second 2-min test trial. Mice were then returned to their respective home cages.

Occlusion experiments—10-week old WT male mice were left to habituate for 30 min in a clean cage before being exposed to a 5-week old juvenile for 2 min. The juvenile was removed and the animal for sacrificed 30 min later. Slices were prepared as indicated above. In order to measure the baseline CA2 FFI we repeated the experiment described above and exposed the recorded mouse either to a novel juvenile or to a littermate for 2 min.

QUANTIFICATION AND STATISTICAL ANALYSIS

Data analysis for electrophysiology—The amplitudes of the PSPs were normalized to the baseline. The magnitude of plasticity was estimated by comparing averaged responses at 30–35 min after the induction protocol with baseline-averaged responses 0–10 min before the induction protocol. All drugs were bath-applied following dilution into the external solution from stock solutions. We used Axograph X software for data acquisition, and Excel (Microsoft) and PRISM (Graphpad) for data analysis. Wilcoxon or Mann-Whitney tests were performed with PRISM for statistical comparisons of paired or non-paired data respectively. Unless stated otherwise, p values come from Mann-Whitney tests. Results presented in the text and figures are reported as the mean ± SEM. * is for $p<0.05$, ** is for $p<0.01$ and *** is for $p<0.001$.

Data analysis for behavior—2-min films were scored offline for social interaction by a trained observer blind to the experimental condition. Sniffing of any part of the body, allogrooming and close following (within 1 cm) of the juvenile counted as social interaction (see on the top right corner of the video when the mention "social" appears). Adults were required to investigate the juveniles for a minimum of 24 s during the initial trial. One mouse did not meet this criterion and was excluded from the analysis. We observed no aggression. Percentage of decline was calculated by dividing the time a mouse interacted during the second trial by the time it interacted during the first trial. Wilcoxon or Mann-Whitney tests were performed with PRISM for statistical comparisons of paired or non-paired data respectively. Results presented in the text and figures are reported as the mean ± SEM. * is for $p<0.05$, ** is for $p<0.01$ and *** is for $p<0.001$.

Supplementary Material

Refer to Web version on PubMed Central for supplementary material.

Acknowledgments

The authors thank Matt Bailey and Eleanor Simpson for their advice with the micro-perfusion system as well as Jung Park for his help preparing the videos. We are also grateful to Thomas Reardon for providing us with the N2C rabies virus and associated glycoprotein expressing rAAV. This work was supported by the R01 MH104602-01 and the Portuguese Foundation for Science and Technology.

References

Alger BE, Teyler TJ. Long-term and short-term plasticity in the CA1, CA3, and dentate regions of the rat hippocampal slice. Brain Res. 1976; 110:463–480. [PubMed: 947467]

Andrioli A, Alonso-Nanclares L, Arellano JI, DeFelipe J. Quantitative analysis of parvalbumin-immunoreactive cells in the human epileptic hippocampus. Neuroscience. 2007; 149:131–143. [PubMed: 17850980]

Basu J, Siegelbaum SA. The Corticohippocampal Circuit, Synaptic Plasticity, and Memory. Cold Spring Harb Perspect Biol. 2015; 7

Basu J, Srinivas KV, Cheung SK, Taniguchi H, Huang ZJ, Siegelbaum SA. A cortico-hippocampal learning rule shapes inhibitory microcircuit activity to enhance hippocampal information flow. Neuron. 2013; 79:1208–1221. [PubMed: 24050406]

Basu J, Zaremba JD, Cheung SK, Hitti FL, Zemelman BV, Losonczy A, Siegelbaum SA. Gating of hippocampal activity, plasticity, and memory by entorhinal cortex long-range inhibition. Science. 2016; 351:aaa5694. [PubMed: 26744409]

Benes FM, Kwok EW, Vincent SL, Todtenkopf MS. A reduction of nonpyramidal cells in sector CA2 of schizophrenics and manic depressives. Biol Psychiatry. 1998; 44:88–97. [PubMed: 9646890]

Blasco-Ibanez JM, Martinez-Guijarro FJ, Freund TF. Enkephalin-containing interneurons are specialized to innervate other interneurons in the hippocampal CA1 region of the rat and guinea-pig. Eur J Neurosci. 1998; 10:1784–1795. [PubMed: 9751150]

Bliss TV, Lomo T. Long-lasting potentiation of synaptic transmission in the dentate area of the anaesthetized rabbit following stimulation of the perforant path. J Physiol. 1973; 232:331–356. [PubMed: 4727084]

Burstein SR, Williams TJ, Lane DA, Knudsen MG, Pickel VM, McEwen BS, Waters EM, Milner TA. The influences of reproductive status and acute stress on the levels of phosphorylated delta opioid receptor immunoreactivity in rat hippocampus. Brain Res. 2013; 1518:71–81. [PubMed: 23583481]

Chavkin C, Bakhit C, Bloom FE. Evidence for dynorphin-A as a neurotransmitter in rat hippocampus. Life Sci. 1983; 33(Suppl 1):13–16. [PubMed: 6141483]

Chavkin C, Shoemaker WJ, McGinty JF, Bayon A, Bloom FE. Characterization of the prodynorphin and proenkephalin neuropeptide systems in rat hippocampus. J Neurosci. 1985; 5:808–816. [PubMed: 3838345]

Chevaleyre V, Castillo PE. Endocannabinoid-mediated metaplasticity in the hippocampus. Neuron. 2004; 43:871–881. [PubMed: 15363397]

Chevaleyre V, Siegelbaum SA. Strong CA2 pyramidal neuron synapses define a powerful disynaptic cortico-hippocampal loop. Neuron. 2010; 66:560–572. [PubMed: 20510860]

Cho JH, Bayazitov IT, Meloni EG, Myers KM, Carlezon WA Jr, Zakharenko SS, Bolshakov VY. Coactivation of thalamic and cortical pathways induces input timing-dependent plasticity in amygdala. Nat Neurosci. 2011; 15:113–122. [PubMed: 22158512]

Chow BY, Han X, Dobry AS, Qian X, Chuong AS, Li M, Henninger MA, Belfort GM, Lin Y, Monahan PE, Boyden ES. High-performance genetically targetable optical neural silencing by light-driven proton pumps. Nature. 2010; 463:98–102. [PubMed: 20054397]

Commons KG, Milner TA. Ultrastructural relationships between leuenkephalin- and GABA-containing neurons differ within the hippocampal formation. Brain Res. 1996; 724:1–15. [PubMed: 8816250]

Csicsvari J, Hirase H, Czurko A, Mamiya A, Buzsaki G. Oscillatory coupling of hippocampal pyramidal cells and interneurons in the behaving Rat. J Neurosci. 1999; 19:274–287. [PubMed: 9870957]

Donato F, Rompani SB, Caroni P. Parvalbumin-expressing basket-cell network plasticity induced by experience regulates adult learning. Nature. 2013; 504:272–276. [PubMed: 24336286]

Dudek SM, Alexander GM, Farris S. Rediscovering area CA2: unique properties and functions. Nat Rev Neurosci. 2016; 17:89–102. [PubMed: 26806628]

Dudman JT, Tsay D, Siegelbaum SA. A role for synaptic inputs at distal dendrites: instructive signals for hippocampal long-term plasticity. Neuron. 2007; 56:866–879. [PubMed: 18054862]

Duka T, Wuster M, Schubert P, Stoiber R, Herz A. Selective localization of different types of opiate receptors in hippocampus as revealed by in vitro autoradiography. Brain Res. 1981; 205:181–186. [PubMed: 6258708]

Erbs E, Faget L, Scherrer G, Kessler P, Hentsch D, Vonesch JL, Matifas A, Kieffer BL, Massotte D. Distribution of delta opioid receptor-expressing neurons in the mouse hippocampus. Neuroscience. 2012; 221:203–213. [PubMed: 22750239]

Frank LM, Brown EN, Wilson MA. A comparison of the firing properties of putative excitatory and inhibitory neurons from CA1 and the entorhinal cortex. J Neurophysiol. 2001; 86:2029–2040. [PubMed: 11600659]

Fuentealba P, Tomioka R, Dalezios Y, Marton LF, Studer M, Rockland K, Klausberger T, Somogyi P. Rhythmically active enkephalin-expressing GABAergic cells in the CA1 area of the hippocampus project to the subiculum and preferentially innervate interneurons. J Neurosci. 2008; 28:10017–10022. [PubMed: 18829959]

Gall C, Brecha N, Karten HJ, Chang KJ. Localization of enkephalin-like immunoreactivity to identified axonal and neuronal populations of the rat hippocampus. J Comp Neurol. 1981; 198:335–350. [PubMed: 6263955]

Hippenmeyer S, Vrieseling E, Sigrist M, Portmann T, Laengle C, Ladle DR, Arber S. A developmental switch in the response of DRG neurons to ETS transcription factor signaling. PLoS Biol. 2005; 3:e159. [PubMed: 15836427]

Hitti FL, Siegelbaum SA. The hippocampal CA2 region is essential for social memory. Nature. 2014; 508:88–92. [PubMed: 24572357]

Ito M. Cerebellar long-term depression: characterization, signal transduction, and functional roles. Physiol Rev. 2001; 81:1143–1195. [PubMed: 11427694]

Jarsky T, Roxin A, Kath WL, Spruston N. Conditional dendritic spike propagation following distal synaptic activation of hippocampal CA1 pyramidal neurons. Nat Neurosci. 2005; 8:1667–1676. [PubMed: 16299501]

Junyent F, Kremer EJ. CAV-2--why a canine virus is a neurobiologist's best friend. Curr Opin Pharmacol. 2015; 24:86–93. [PubMed: 26298516]

Kitamura T, Pignatelli M, Suh J, Kohara K, Yoshiki A, Abe K, Tonegawa S. Island cells control temporal association memory. Science. 2014; 343:896–901. [PubMed: 24457215]

Kogan JH, Frankland PW, Silva AJ. Long-term memory underlying hippocampus-dependent social recognition in mice. Hippocampus. 2000; 10:47–56. [PubMed: 10706216]

Kohara K, Pignatelli M, Rivest AJ, Jung HY, Kitamura T, Suh J, Frank D, Kajikawa K, Mise N, Obata Y, et al. Cell type-specific genetic and optogenetic tools reveal hippocampal CA2 circuits. Nat Neurosci. 2014; 17:269–279. [PubMed: 24336151]

Kowalski J, Gan J, Jonas P, Pernia-Andrade AJ. Intrinsic membrane properties determine hippocampal differential firing pattern in vivo in anesthetized rats. Hippocampus. 2015

McGinty JF, Henriksen SJ, Goldstein A, Terenius L, Bloom FE. Dynorphin is contained within hippocampal mossy fibers: immunochemical alterations after kainic acid administration and colchicine-induced neurotoxicity. Proc Natl Acad Sci U S A. 1983; 80:589–593. [PubMed: 6132379]

Mercer A, Botcher NA, Eastlake K, Thomson AM. SP-SR interneurones: a novel class of neurones of the CA2 region of the hippocampus. Hippocampus. 2012; 22:1758–1769. [PubMed: 22431345]

Mercer A, Trigg HL, Thomson AM. Characterization of neurons in the CA2 subfield of the adult rat hippocampus. J Neurosci. 2007; 27:7329–7338. [PubMed: 17611285]

Nasrallah K, Piskorowski RA, Chevaleyre V. Inhibitory Plasticity Permits the Recruitment of CA2 Pyramidal Neurons by CA3(1,2,3). eNeuro. 2015; 2

Nasrallah K, Piskorowski RA, Chevaleyre V. Bi-directional interplay between proximal and distal inputs to CA2 pyramidal neurons. Neurobiol Learn Mem. 2016

Ognjanovski N, Schaeffer S, Wu J, Mofakham S, Maruyama D, Zochowski M, Aton SJ. Parvalbumin-expressing interneurons coordinate hippocampal network dynamics required for memory consolidation. Nat Commun. 2017; 8:15039. [PubMed: 28382952]

Okuyama T, Kitamura T, Roy DS, Itohara S, Tonegawa S. Ventral CA1 neurons store social memory. Science. 2016; 353:1536–1541. [PubMed: 27708103]

Pagani JH, Zhao M, Cui Z, Avram SK, Caruana DA, Dudek SM, Young WS. Role of the vasopressin 1b receptor in rodent aggressive behavior and synaptic plasticity in hippocampal area CA2. Mol Psychiatry. 2015; 20:490–499. [PubMed: 24863146]

Piskorowski RA, Chevaleyre V. Delta-opioid receptors mediate unique plasticity onto parvalbumin-expressing interneurons in area CA2 of the hippocampus. J Neurosci. 2013; 33:14567–14578. [PubMed: 24005307]

Piskorowski RA, Nasrallah K, Diamantopoulou A, Mukai J, Hassan SI, Siegelbaum SA, Gogos JA, Chevaleyre V. Age-Dependent Specific Changes in Area CA2 of the Hippocampus and Social Memory Deficit in a Mouse Model of the 22q11.2 Deletion Syndrome. Neuron. 2016; 89:163–176. [PubMed: 26748091]

Reardon TR, Murray AJ, Turi GF, Wirblich C, Croce KR, Schnell MJ, Jessell TM, Losonczy A. Rabies Virus CVS-N2c(DeltaG) Strain Enhances Retrograde Synaptic Transfer and Neuronal Viability. Neuron. 2016; 89:711–724. [PubMed: 26804990]

Ribak CE, Seress L, Leranth C. Electron microscopic immunocytochemical study of the distribution of parvalbumin-containing neurons and axon terminals in the primate dentate gyrus and Ammon's horn. J Comp Neurol. 1993; 327:298–321. [PubMed: 8425946]

Safo P, Regehr WG. Timing dependence of the induction of cerebellar LTD. Neuropharmacology. 2008; 54:213–218. [PubMed: 17669443]

Sar M, Stumpf WE, Miller RJ, Chang KJ, Cuatrecasas P. Immunohistochemical localization of enkephalin in rat brain and spinal cord. J Comp Neurol. 1978; 182:17–37. [PubMed: 359601]

Simmons ML, Chavkin C. Endogenous opioid regulation of hippocampal function. Int Rev Neurobiol. 1996; 39:145–196. [PubMed: 8894847]

Smith AS, Williams Avram SK, Cymerblit-Sabba A, Song J, Young WS. Targeted activation of the hippocampal CA2 area strongly enhances social memory. Mol Psychiatry. 2016

Stevenson EL, Caldwell HK. Lesions to the CA2 region of the hippocampus impair social memory in mice. Eur J Neurosci. 2014; 40:3294–3301. [PubMed: 25131412]

Stumm RK, Zhou C, Schulz S, Hollt V. Neuronal types expressing mu- and delta-opioid receptor mRNA in the rat hippocampal formation. J Comp Neurol. 2004; 469:107–118. [PubMed: 14689476]

Svoboda KR, Adams CE, Lupica CR. Opioid receptor subtype expression defines morphologically distinct classes of hippocampal interneurons. J Neurosci. 1999; 19:85–95. [PubMed: 9870941]

Takahashi H, Magee JC. Pathway interactions and synaptic plasticity in the dendritic tuft regions of CA1 pyramidal neurons. Neuron. 2009; 62:102–111. [PubMed: 19376070]

Terrian DM, Johnston D, Claiborne BJ, Ansah-Yiadom R, Strittmatter WJ, Rea MA. Glutamate and dynorphin release from a subcellular fraction enriched in hippocampal mossy fiber synaptosomes. Brain Res Bull. 1988; 21:343–351. [PubMed: 2905627]

Urban DJ, Roth BL. DREADDs (designer receptors exclusively activated by designer drugs): chemogenetic tools with therapeutic utility. Annu Rev Pharmacol Toxicol. 2015; 55:399–417. [PubMed: 25292433]

van den Pol AN. Neuropeptide transmission in brain circuits. Neuron. 2012; 76:98–115. [PubMed: 23040809]

Wall NR, Wickersham IR, Cetin A, De La Parra M, Callaway EM. Monosynaptic circuit tracing in vivo through Cre-dependent targeting and complementation of modified rabies virus. Proc Natl Acad Sci U S A. 2010; 107:21848–21853. [PubMed: 21115815]

Xu JY, Zhang J, Chen C. Long-lasting potentiation of hippocampal synaptic transmission by direct cortical input is mediated via endocannabinoids. J Physiol. 2012; 590:2305–2315. [PubMed: 22411015]

Yeckel MF, Berger TW. Feedforward excitation of the hippocampus by afferents from the entorhinal cortex: redefinition of the role of the trisynaptic pathway. Proc Natl Acad Sci U S A. 1990; 87:5832–5836. [PubMed: 2377621]

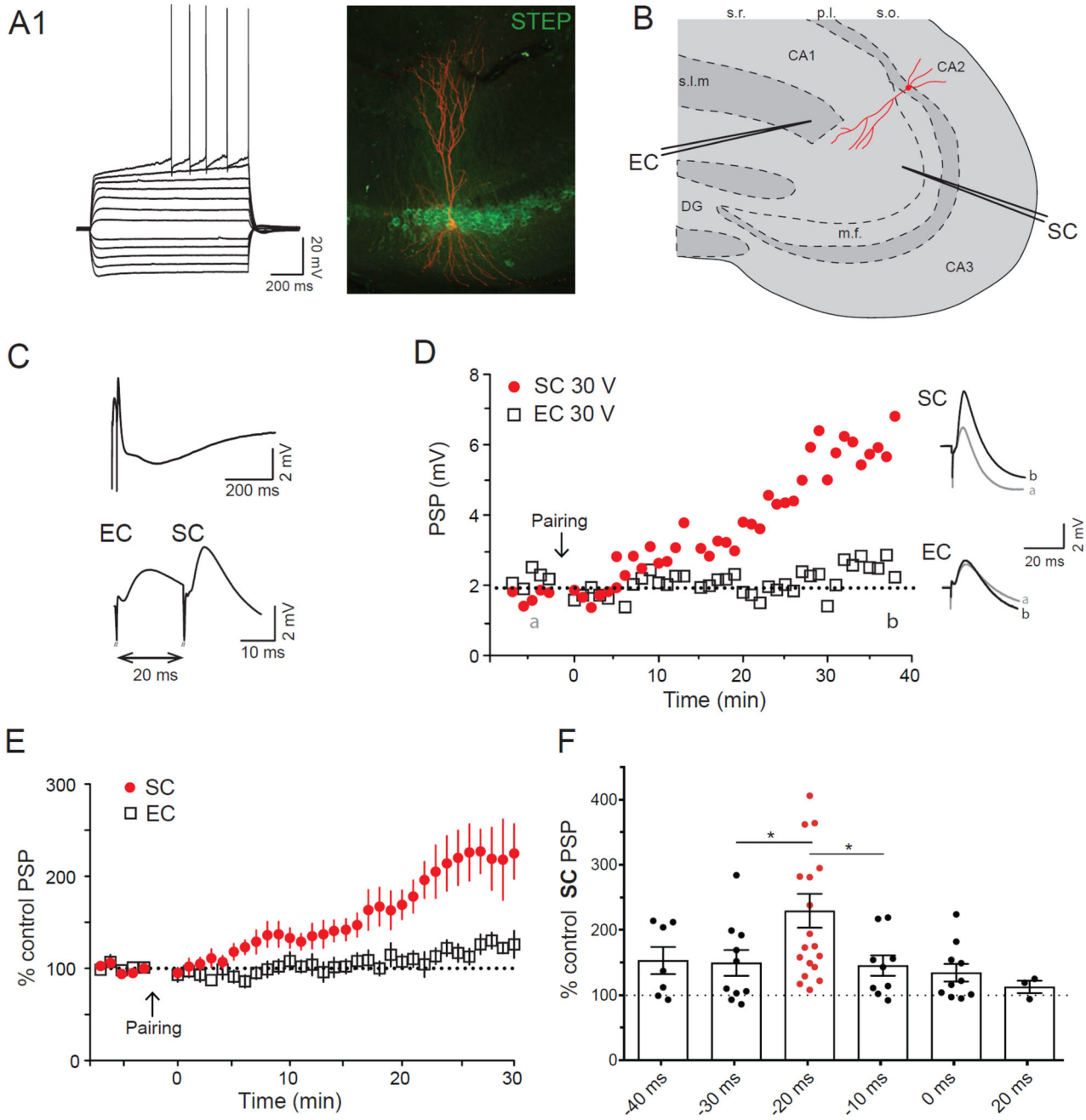

Figure 1. CA2 PNs display ITDP

A1. Whole-cell current-clamp recording following injection of 25 pA current steps. **A2**. Streptavidin (red) and STEP (green) immunohistochemistry of the biocytin filled PN. **B**. Drawing of the localization of the stimulating electrodes in the hippocampal slice. **C**. Current-clamp response during the ITDP induction protocol (repeated 90 times at 1 Hz). The bottom trace is an enlargement of the upper one. **D**. Time course of the EC and SC PSPs amplitudes obtained in current-clamp following ITDP induction (left). On the right are displayed the SC and EC PSP before (grey) and after (black) ITDP. Data from **A** to **C** (and from Supplementary figure 1S1) is from the same CA2 PN. **E**. Time course of the average

normalized PSPs amplitudes obtained in whole-cell current-clamp following ITDP induction. **F**. Normalized SC PSP amplitudes following ITDP induction using different intervals between the EC and SC stimulation (−20ms indicate EC followed by the SC 20ms later). Data are represented as mean ± SEM. See also Figure S1.

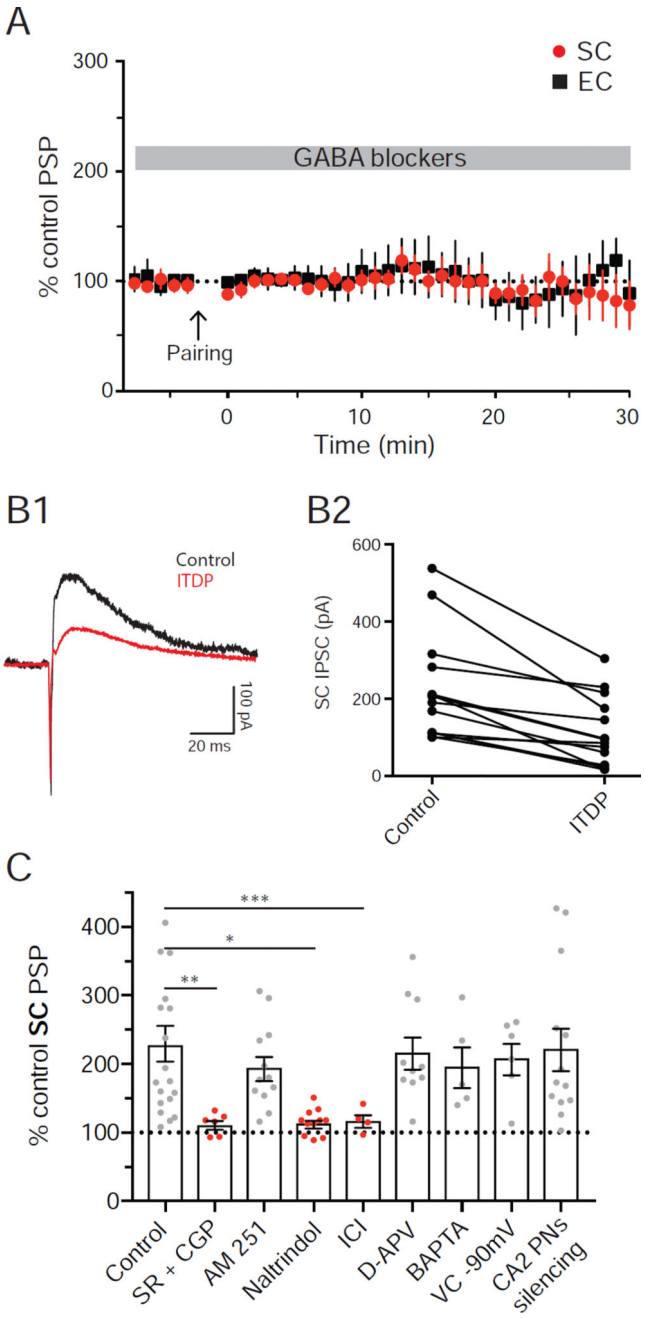

Figure 2. Mechanisms of ITDP in CA2 PNs

A. Time course of the average normalized PSPs amplitudes obtained in whole-cell current-clamp following ITDP induction in the presence of GABA blockers. **B**. Whole-cell voltage-clamp recordings of CA2 PNs IPSCs at a holding potential of −10 mV. IPSCs are induced by SC stimulation (**B1**). Amplitude of the SC IPSCs is compared before and after ITDP (**B2**). Empty circle is the cell shown in **B1. C.** Normalized SC PSP amplitudes following ITDP induction in the presence of different drugs or with the CA2 PNs silenced by inhibitory DREADDs. Data are represented as mean ± SEM. See also Figure S2.

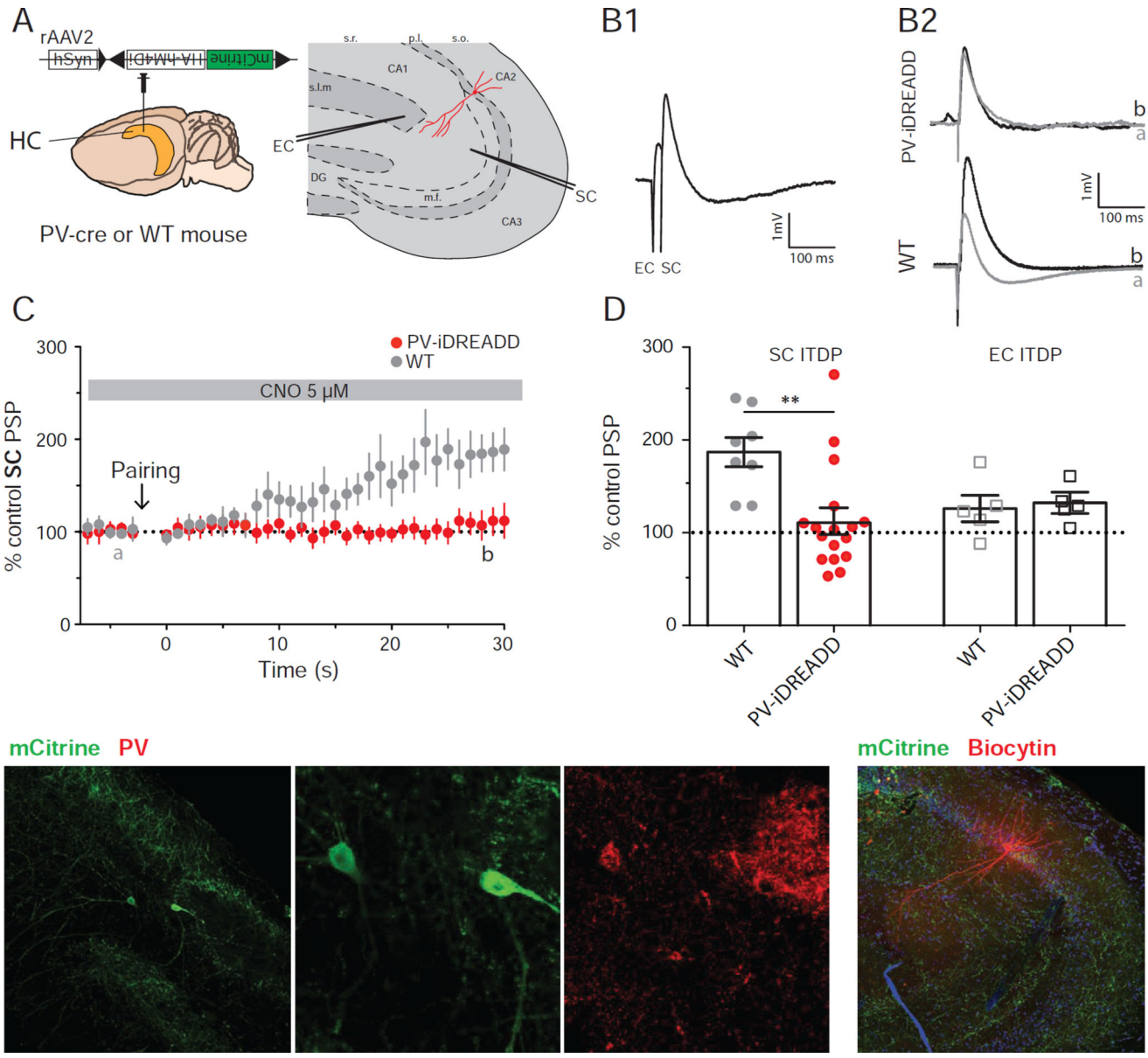

Figure 3. PV+ IN population is necessary for ITDP expression

A. Experimental design showing injection of Cre-dependent iDREADD virus in PV-Cre or WT mouse. **B:** PSPs recorded in whole-cell current-clamp configuration in response to paired electrical stimulation of EC+SC inputs (**B1**) or SC inputs alone (**B2**) from neurons in slices from PV-Cre mouse expressing iDREADD or WT mouse injected with same virus (no iDREADD expression). **B1.** Example paired EC+SC PSPs from neuron in iDREAD-Dexpressing slice. **B2.** SC-evoked PSPs before (black) and 30 min after (grey) ITDP induction. **C.** Time course of mean ± SEM SC PSP amplitude during ITDP. **D:** SC (filled circles) and EC (open squares) PSP amplitude following ITDP induction using electrical pairing in WT or PV-Cre mice, both injected with iDREADD. Symbols show data for single cells; bars show mean ± SEM. **E**. Immunohistochemistry of acute hippocampal slice showing mCitrine (from Cre-dependent virus) and PV expression. **F**. Immunohistochemistry

of acute hippocampal slice showing mCitrine and biocytin-filled neuron. See also Figures S3 and S4.

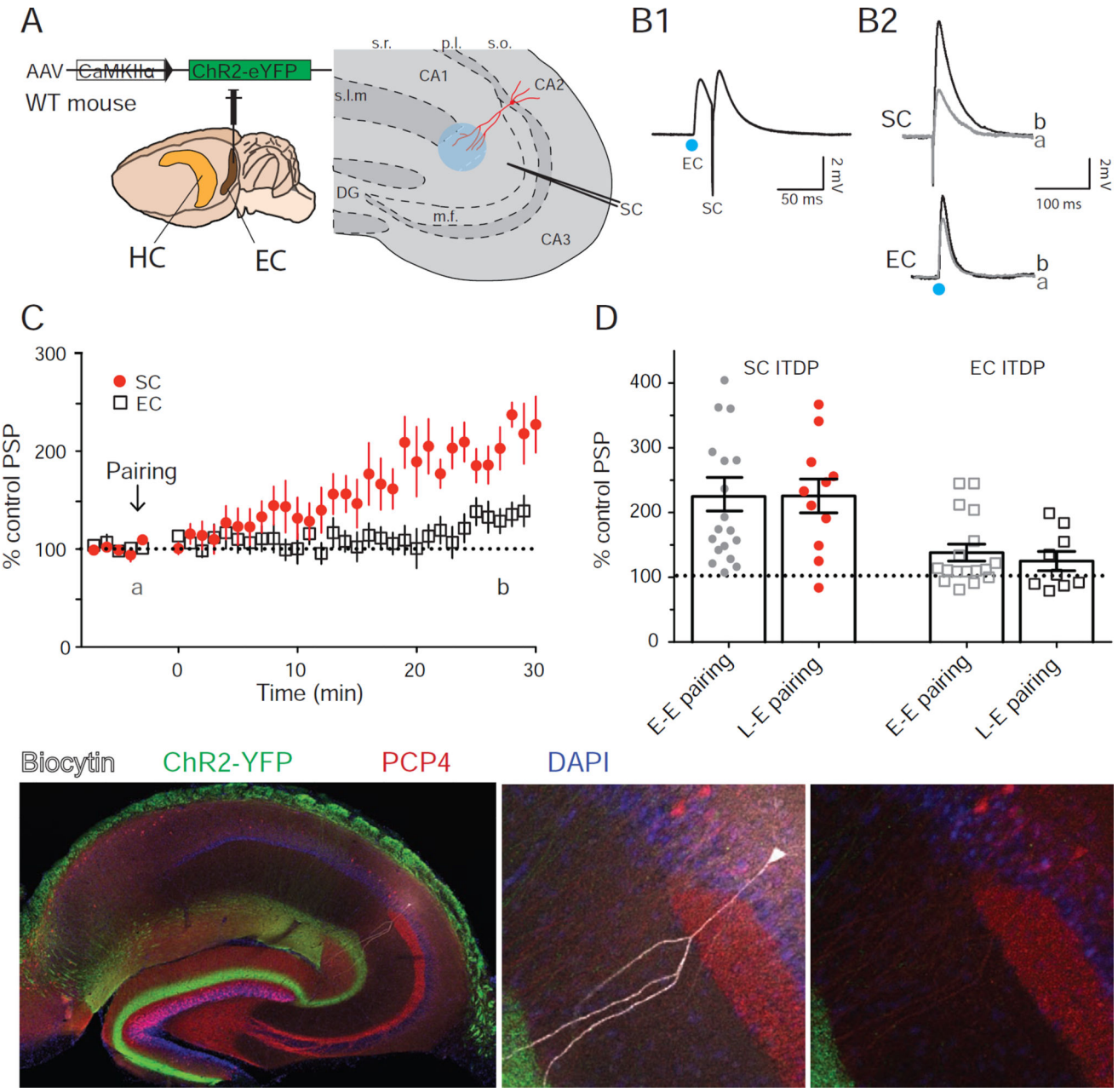

Figure 4. Pairing light-stimulation of the MEC excitatory inputs with SC stimulation also induces ITDP in CA2

A. Experimental design of the experiment and injection site of the channelrhodopsin expressing virus. **B.** Responses obtained in whole-cell current-clamp configuration using light (EC) or electrical (SC) stimulations during ITDP induction (**B1**) or during the time course (**B2**) before (black) and 30 min after (grey) ITDP induction. **C.** Time course of PSPs amplitudes during ITDP. **D.** Normalized SC (filled circles) and EC (open squares) PSPs amplitudes following ITDP induced using electrical-electrical or light-electrical pairing. Symbols show data for single cells; bars show mean ± S.E.M. **E**. Immunohistochemistry of the acute hippocampal slice against biocytin, ChR2-YFP, PCP4. Arrowhead in **E3** indicates

the PCP4 positive soma of the recorded cell. Data from **B** and **E** is from the same CA2 PN. See also Figure S5.

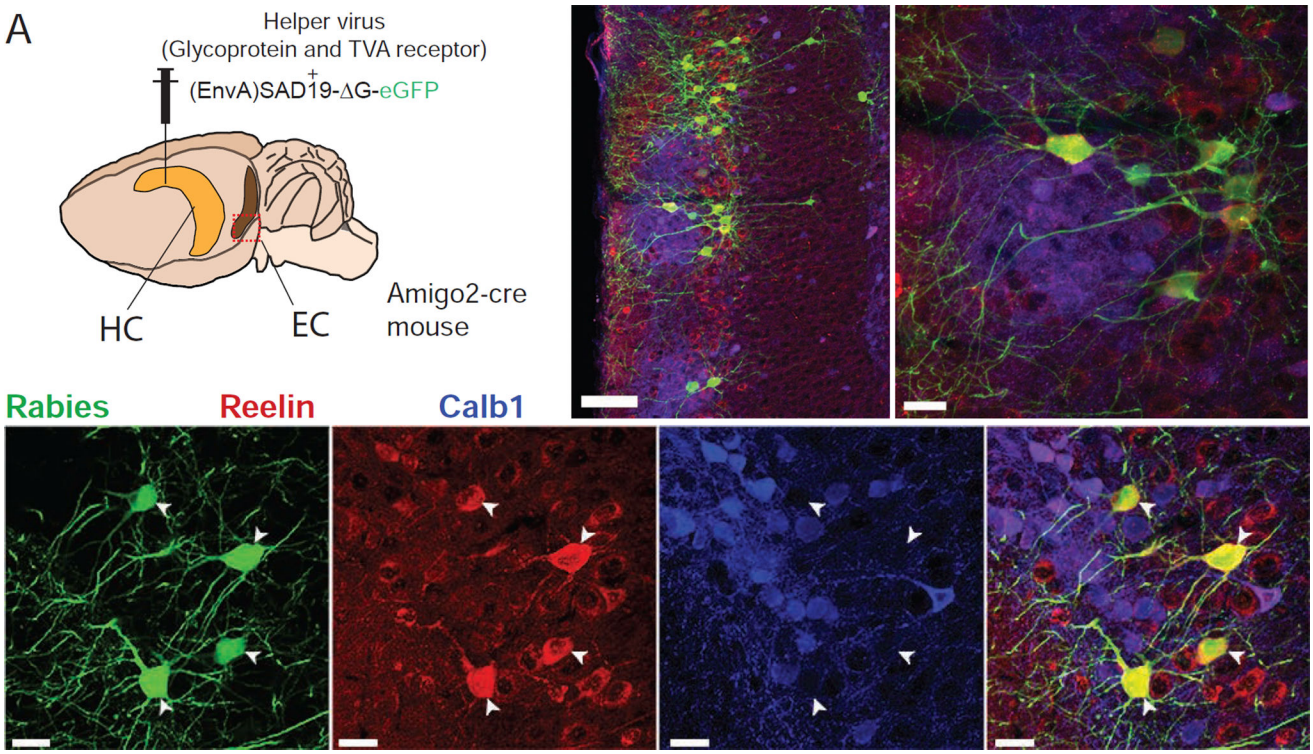

Figure 5. CA2 direct EC inputs originates from the EC LII stellate cells

A. Experimental design and injection site of the helper and Rabies viruses. **B–C.** Immunohistochemistry of the MEC (**B**) and LEC (**C**) against Rabies-YFP, Calb1 and Reelin. See also Figure S6.

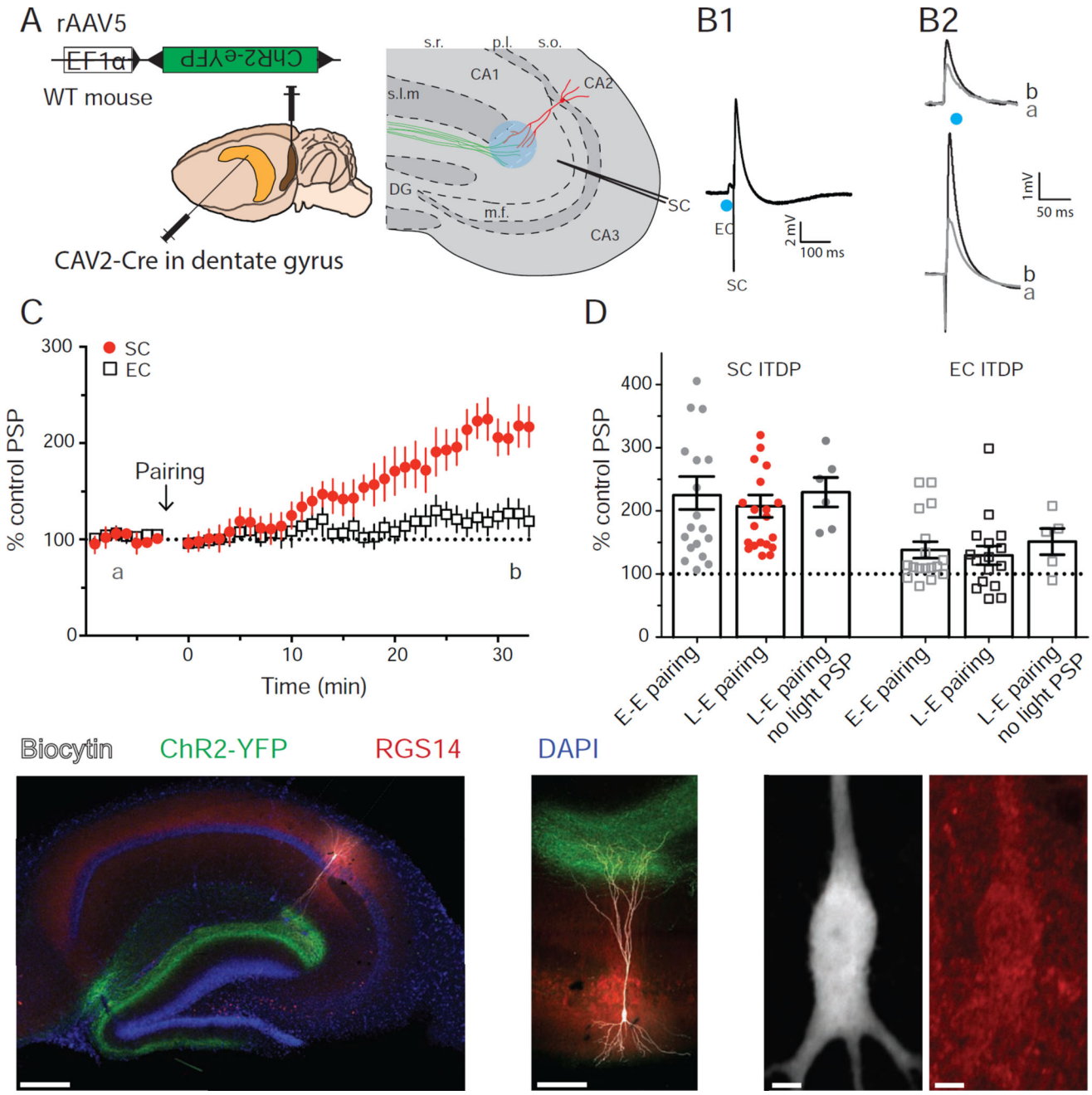

Figure 6. Pairing photo-stimulation of LEC LII stellate cells inputs with SC electrical stimulation induces ITDP in CA2

A. Experimental design and injection sites of CAV2-Cre in DG and Cre-dependent ChR2 rAAV in EC. **B.** CA2 PN PSPs from whole-cell current-clamp recordings. (**B1**) PSPs evoked using paired light (EC) and electrical (SC) stimulation during ITDP induction. (**B2**) Light-evoked EC PSPs (top) and electrically evoked SC PSPs before (black) and 30 min after (grey) ITDP induction. **C.** Time course of mean ± SEM peak PSP amplitude during ITDP. **D.** SC (filled circles) and EC (open squares) PSP amplitudes normalized by baseline showing ITDP induced by pairing electrical stimulation of the SC input with electrical (E-E) or light

(L-E) stimulation of the EC input. Results for ITDP in cells that showed no light-evoked EC PSP are also shown (L-E pairing, no light PSP). Symbols show data for single cells; bars show mean ± SEM. **E**. Immunohistochemistry from hippocampal slices against YFP, Biocytin and RGS14. **E1.** Whole slice. **E2.** Expanded view of the recorded cell morphology. **E3**. High magnification view of the soma of the recorded cell (left, biocytin image) to confirm the expression of the CA2 marker RGS14 (right, red). See also Figure S7.

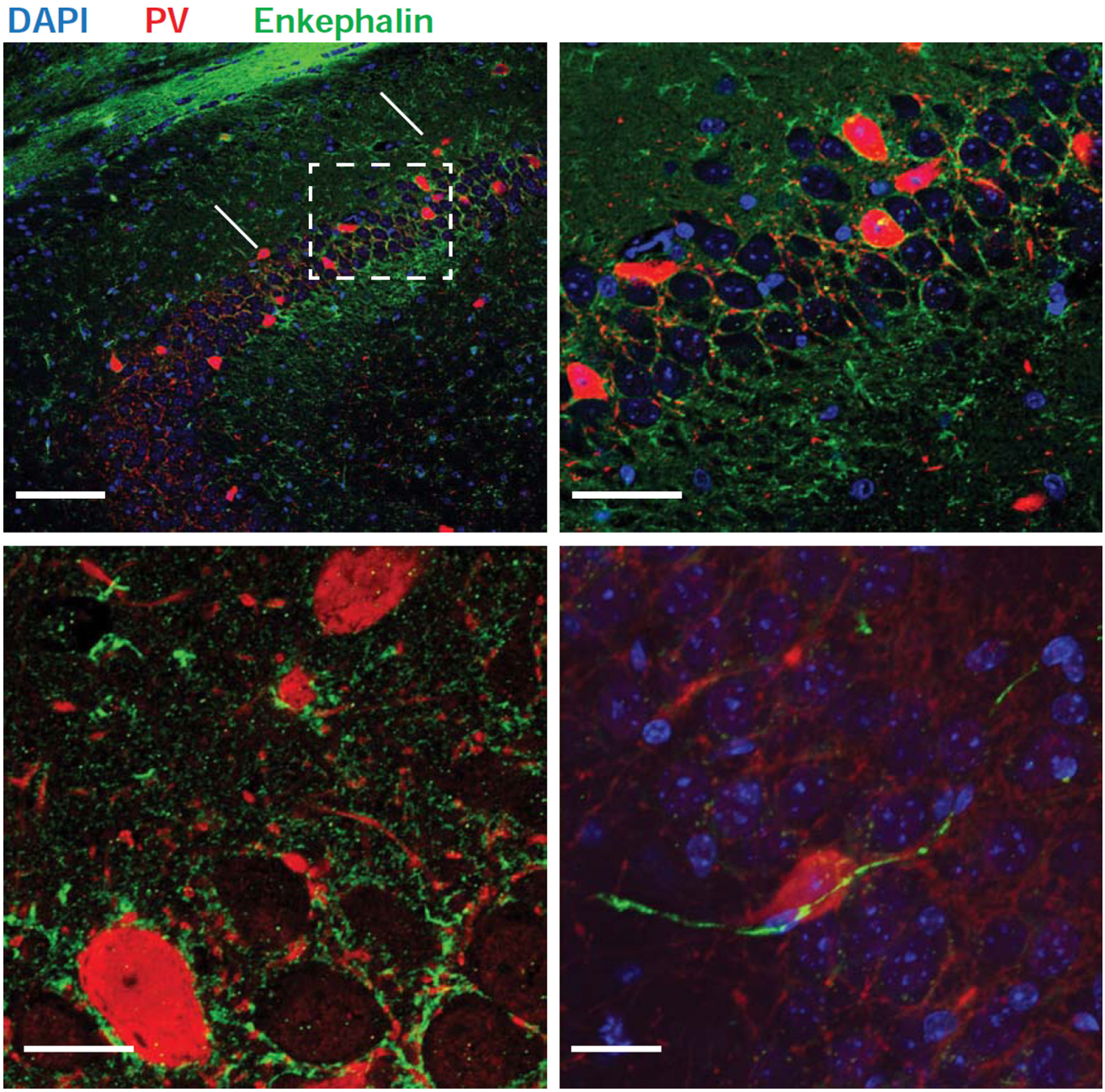

Figure 7. ENK$^+$ fibers contact PV$^+$ INs

A–C. Immunohistochemistry of the hippocampus with antibodies recognizing PV (red) and enkephalin (green). Fitzgerald enkephalin antibody used in **A** and **B;** Santa Cruz enkephalin antibody used in **C;** see Experimental Procedures. Arrowhead in **A1** points to the end of the mossy fiber pathway. **A2.** Higher magnification view of dashed box region in **A1**. **B**. High magnification view of the tight network of ENK$^+$ (green) and PV$^+$ fibers (red) surrounding unstained CA2 PNs somas (asterisks). Two PV$^+$ neuron somas are also seen (large red somas). In **C,** an ENK$^+$ fiber can be seen impinging on a PV$^+$ soma.

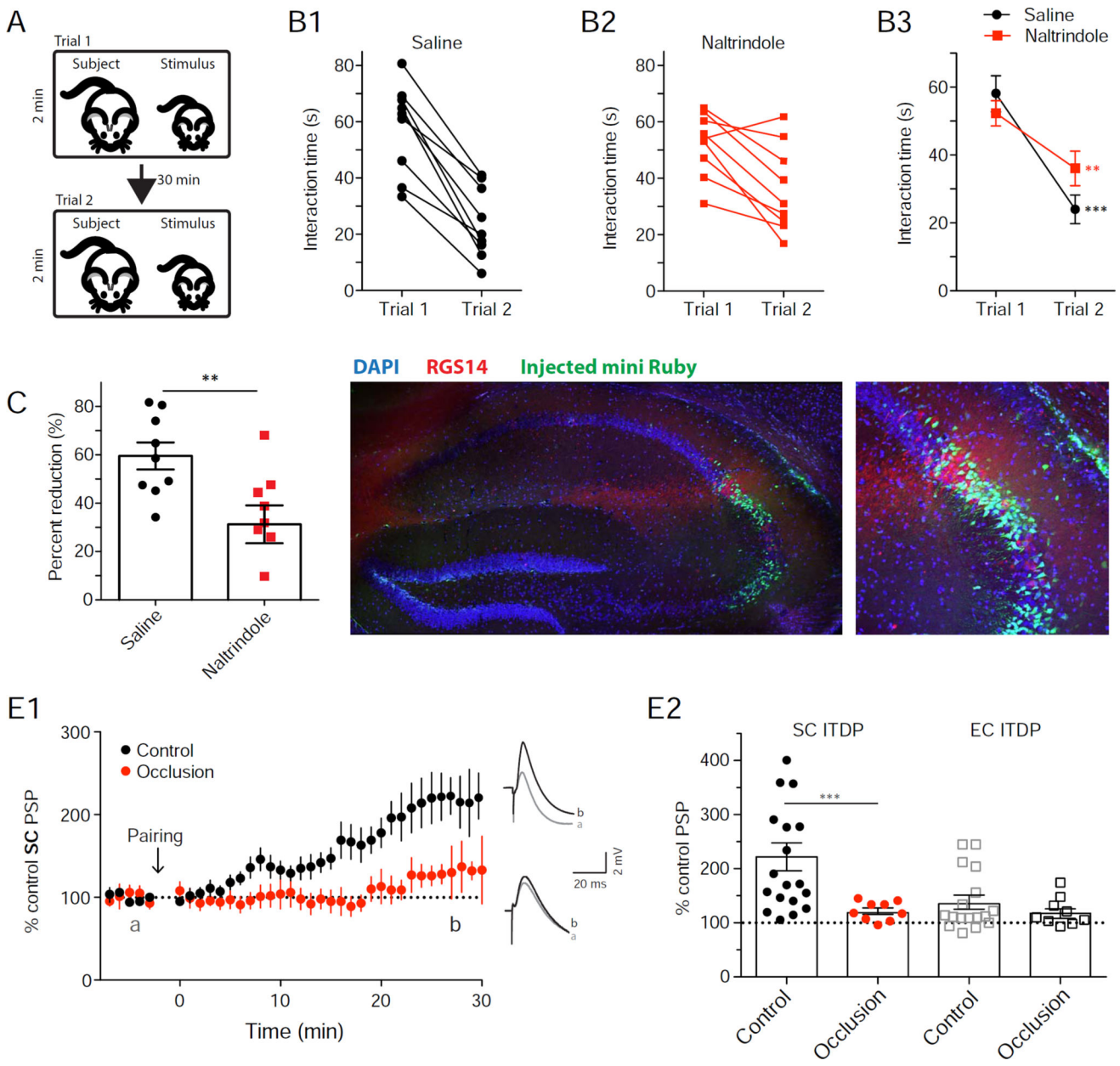

Figure 8. DOR blockade in CA2 reduces social memory and social memory occludes ITDP

A. Schematic of the direct interaction test for social memory. **B**. Interaction time of saline (**B1**) and naltrindole-injected (**B2**) animals in trials 1 and 2 (symbols from individual animals) and superimposed mean ± SEM data (**B3**). **C.** Percent reduction of interaction time from trial 1 to trial 2. **D**. Mini-Ruby infusion in the hippocampus and immunohistochemistry for RGS14. **E**. Time course of mean ± SEM normalized SC PSP amplitude obtained in whole-cell current-clamp following ITDP induction. Slices were prepared from mice that either experienced a 2-min interaction with a novel juvenile male (social novelty) or were continuously housed with littermates (social familiarity). Note pronounced reduction in ITDP in response to social novelty **D.** ITDP of PSPs evoked by stimulation of SC (filled

circles) or EC (open squares) inputs to CA2 PNs in slices from indicated groups of animals. Symbols show data for single cells; bars show mean ± SEM. See also Figure S8.